PARP-1: A novel nuclear polyphosphoinositide effector protein

Malene Skuseth Slinning

This thesis is submitted in partial fulfilment of the requirements for the degree of Master of Science

Department of Biological Sciences
Faculty of Mathematics and Natural Sciences
University of Bergen

June 2020

Acknowledgments

The work presented in this thesis was performed at the Department of Biological Sciences, University of Bergen, in the period August 2019 to May 2020.

First and foremost, I would like to thank my supervisor, associate professor Aurélia E. Lewis for all your help and guidance. Thank you for always taking your time to answer my questions, for all the nice talks and for all the great feedbacks when writing my thesis.

I would also like to give a special thanks to by co-supervisor, Diana C. Turcu. I am so grateful for everything you have taught me in the lab and for always helping me whenever I have needed it. Thank you for all the nice conversations and all the troubleshooting, when my cloning didn´t work.

I would also like to thank everyone else in the NUCREG group and the rest of the people at MOL-BIO. It has been a joy to work with all of you. A special thanks to Grethe Aarbakke for giving me the opportunity to teach. I also want to thank my fellow master students for all the fun times we have had together during the master.

A huge thanks to my family and friends for all the support and love you have given me over the past five years. It has meant so much to me. Lastly, a special thanks to my boyfriend, Joakim, for always believing in me and motivating me. I am so grateful for all your help and support when writing this thesis. I couldn´t have done this without you.

Table of contents

Selected abbreviations

AD	Automodification domain
BER	Base excision repair
DBD	DNA binding domain
DSB	Double strand break
HR	Homologous recombination
K/R motif	Lysine/arginine rich motif
MEF	Mouse embryonic fibroblast
NHEJ	Nonhomologous end joining
NLS	Nuclear localization signal
NoD	Nucleolar localization sequence detector
NoLS	Nucleolar localization signal
NPM	Nucleophosmin
P110β	Class I PI3K catalytic isoform β
PAR	Poly(ADP-ribose)
PARP	Poly(ADP-ribose) polymerase
PBR	Polybasic region
PH domain	Pleckstrin homology domain
PI3K	Phosphoinositide 3-Kinase
PIP_3	PtdIns(3,4,5)P_3
PPIn	Polyphosphoinositide
PtdIns	Phosphatidylinositol
rRNA	Ribosomal RNA
SSB	Single strand break

Abstract

Polyphosphoinositides (PPIns) are a family of seven signalling lipids that are important for many cellular processes. While their functional roles in the cytoplasm have been extensively studied, their roles in the nucleus are still poorly understood. To date, several members of the PI3K pathway have been identified within the nucleus, where they have shown to be involved in several nuclear functions such as DNA replication, DNA double strand break repair, and ribosome biogenesis. Previously, our group identified the class I PI3K p110β and its lipid product, PtdIns(3,4,5)P_3 (PIP_3) in the nucleoplasm and the nucleolus. To better understand the nuclear functions of PIP_3, a nuclear PIP_3 interactome was mapped using nuclear extracts from HeLa cells. Interestingly, many of the identified PIP_3 binding proteins were annotated to the nucleolus, a subnuclear structure which is known as the site of ribosome biogenesis. Poly(ADP-ribose) polymerase-1 (PARP-1), an abundant nuclear protein involved in DNA repair and enriched in the nucleolus, was identified as a potential PIP_3 binding protein. This was further confirmed by *in vitro* binding of PARP-1 to PPIns, including PIP_3. Moreover, PARP-1 was shown to co-localize with PIP_3 in the nucleolus in HeLa cells. In the present study, we aimed to determine the specific PIP_3 interaction sites of PARP-1. We showed that PARP-1 binds to PPIns including PIP_3 via two polybasic regions (PBRs) and through binding of one reverse K/R motif, as deletion of either of the PBRs or mutations in the K/R motif reduced or completely abolished all binding to PPIns. PARP-1 has been shown to be localized to the nucleolus, however no nucleolar localization signal has been determined so far. Using the nucleolar sequence detector (NoD) algorithm, we identified that one of the PPIn- binding sites could also act as a potential NoLS. Finally, we wanted to investigate whether PIP_3 is important for the regulation of PARP-1 activity upon H_2O_2 induced DNA damage using MEF cells harbouring WT or kinase dead version of class I PI3K p110β. However, no differences were observed when comparing the PAR-intensities in the two cell lines. Taken together, these results further verify that PARP-1 is a novel PPIn effector protein, however, additional studies must be performed to map their functional role.

1 Introduction

1.1 Polyphosphoinositides

1.1.1 Polyphosphoinositides chemical structure

Lipids are a major group of biomolecules important for many biological processes including cell signalling, energy storage, and as building blocks for cellular membranes (de Carvalho and Caramujo, 2018). Polyphosphoinositides (PPIns) are a small group of signalling lipids comprising less than 1% of total cellular phospholipids, but still are essential in many cellular processes such as membrane dynamics, cytoskeletal rearrangement, ion channel regulation, and signal transduction (De Craene et al., 2017, McCrea and De Camilli, 2009). PPIns derive from phosphatidylinositol (PtdIns), which is a phospholipid comprising two fatty acyl chains that are bound to a glycerol backbone, and a myo-inositol headgroup that is linked to the backbone through a phosphodiester linkage (Balla, 2013) (Figure 1.1). The fatty acid composition of PtdIns consists predominantly of a stearic acid (18:0) linked to position sn-1, and an arachidonic acid (20:4) linked to position sn-2, but other combinations have been observed as well (Barneda et al., 2019). Furthermore, the myo-inositol ring at position sn-3 can be reversibly phosphorylated at the 3′- , 4′-, and 5′- hydroxyl groups yielding a total of 7 different PPIns, including mono-phosphorylated (PtdIns3*P*, PtdIns4*P*, PtdIns5*P*), di-phosphorylated (PtdIns(3,4)P_2, PtdIns(3,5)P_2, PtdIns(4,5)P_2) and tri-phosphorylated (PtdIns(3,4,5)P_3) PPIns (Balla, 2013). The PPIns can act directly as secondary messengers or as precursors in signal transduction pathways (Balla, 2013).

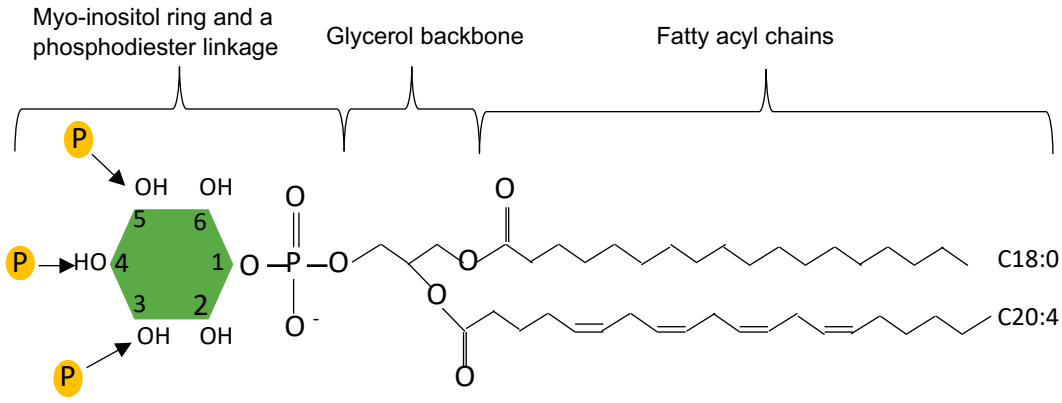

Figure 1.1: Structural overview of phosphatidylinositol (PtdIns). PtdIns comprises two fatty acyl chains (here; C18:0,C20:4) bound to a glycerol backbone and a myo-inositol headgroup linked to the backbone via a phosphodiester linkage. PdtIns can be reversibly phosphorylated by specific phosphoinositide kinases and phosphatases at the 3′-, 4′- and 5′- hydroxyl groups yielding a total of 7 different polyphosphoinositides (PPIns).

1.1.2 Polyphosphoinositide metabolism and localization

The various PPIns are distributed to distinct cellular membrane compartments and their levels are tightly regulated by specific phosphoinositide kinases and phosphatases which add or remove phosphates, respectively (Di Paolo and De Camilli, 2006) (Figure 1.2A). In addition, PtdIns(4,5)P_2 can be hydrolysed by phospholipase C (PLC) yielding the secondary messengers Ins(1,4,5)P_3 and diacylglycerol (DAG) (Balla, 2013).

PtdIns is localized to the endoplasmic reticulum (ER) where it is synthesized by PtdIns synthase (PIS) that uses myo-inositol and cytidine diphosphate diacylglycerol (CDP-DAG) as substrates (Blunsom and Cockcroft, 2020). Following its synthesis, PtdIns is transported to other cellular membrane compartments via either vesicular transport, PI-transfer proteins (PITPs) or via PIS containing vesicles, where it is metabolized to other PPIns (Blunsom and Cockcroft, 2020). PtdIns(3,4)P_2, PtdIns(4,5)P_2 and PtdIns(3,4,5)P_3 are mainly found at the plasma membrane (PM), while PtdIns4P and PtdIns5P are mostly found at the PM and the Golgi apparatus. Moreover, PtdIns3P and PtdIns(3,5)P are found at early endosomes and late endosomes/multivesicular bodies (MVB), respectively (Figure 1.2B). In addition, PPIns have also been reported in the nucleus (De Craene et al., 2017, Viaud et al., 2016)

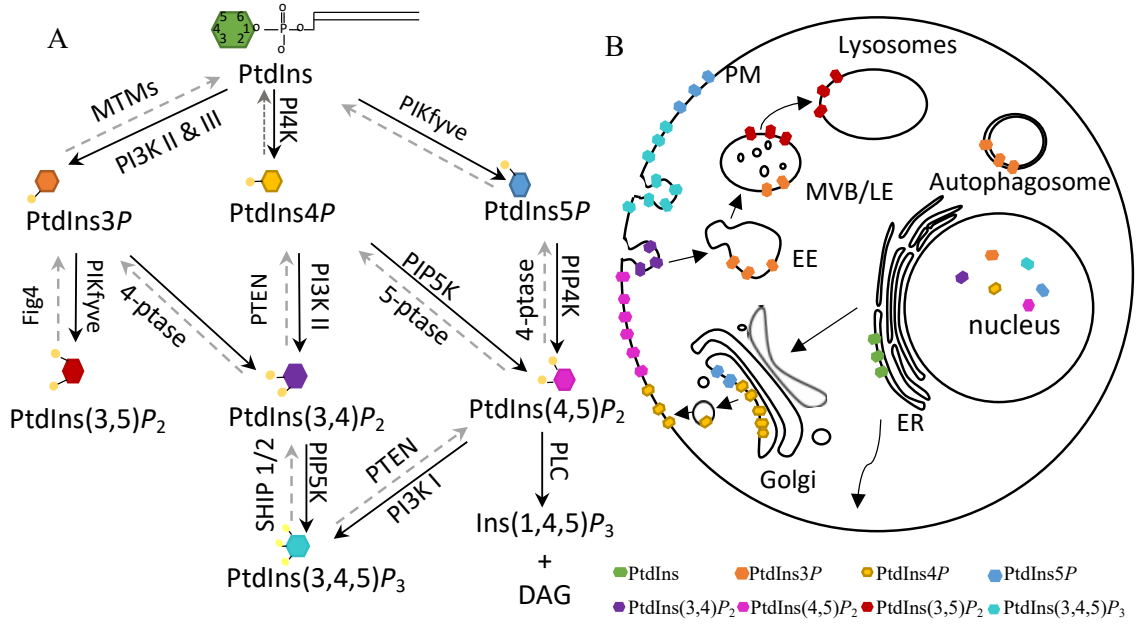

Figure 1.2: Polyphosphoinositide metabolism and localization. A) Overview of the phosphoinositide kinases (black arrow) and phosphatases (grey and dashed arrow) that catalyze the formation of the distinct polyphosphoinositides (PPIns) **B)** Simplified overview of the main localization sites of PPIns. PPIns are also found at other sites than shown, but in smaller pools. Abbreviations: PtdIns: phosphatidylinositol, PI3K: phosphoinositide 3-kinase, PI4K: phosphatidylinositol 4-kinase, PIP4K: phosphatidylinositol 5-phosphate 4-kinase, PIP5K: Phosphatidylinositol-4-phosphate 5-kinases, MTM: myotubularin SHIP: Src homology 2 (SH2) domain-containing inositol 5´phosphatase, PTEN: phosphatase and tensin homolog, DAG: diacylglycerol, PLC: phospholipase C, ptase: phosphatase, EE: early endosomes, MVB: multivesicular bodies, LE: late endosomes, ER: endoplasmic reticulum, PM: plasma membrane.

1.1.3 Polyphosphoinositide-protein mode of interaction

PPIns have their fatty acyl chains embedded in the cellular membrane, while their inositol head groups are exposed into the cytoplasm. In response to stimuli, PPIns recruit proteins to their sub-cellular membranes via specific PPIn-binding domains, or via polybasic motifs through electrostatic interactions (Hammond and Balla, 2015). They interact with proteins essential for many downstream signalling pathways, and dysregulation of PPIn metabolism is seen in a variety of cancers and other diseases such as Lowe´s syndrome and Parkinson's (Staiano et al., 2015, De Craene et al., 2017).

Studies have identified several PPIn-binding domains such as the PH (pleckstrin homology), PX (phox homology), ENTH (Epsin N-terminal homology), FYVE (Fab1, YOTB, Vac1, EEA1), and FERM (band 4.1, ezrin, radixin and moesin) domains (Cullen et al., 2001, Pemberton and Balla, 2018). These are highly conserved and folded domains that show various specificity and affinity for different PPIns (Cullen et al., 2001, Balla, 2013). In addition, PPIns bind proteins via unstructured motifs rich in basic amino acids such as lysine and arginine residues (Martin, 1998). Several PPIn-binding proteins that contain clusters of basic amino acids or K/R motifs following the consensus sequence K/R-(X_{3-7})-K-X-K/R-K/R have been identified (Martin, 1998, Lewis et al., 2011). This K/R motif was originally found in the actin-binding protein gelsolin and other members of the gelsolin family such as villin, Cofilin and Profilin harbour K/R motifs that binds PPIns (Martin, 1998, Yu et al., 1992). Other PPIn-binding proteins such as N-WASP (neuronal Wiskott-Aldrich Syndrom Protein), MARCKS (myristoylated alanine-rich c-kinase substrate), c-Src (cellular-sarcoma non receptor protein tyrosine kinase), and K-Ras (Kirstin-rat sarcoma), to name a few, bind PPIns via unstructured polybasic regions (PBRs) (Papayannopoulos et al., 2005, Pemberton and Balla, 2018).

1.1.4 Polyphosphoinositides in the nucleus

The functional roles of PPIns have been extensively studied in the cytoplasm, however, their activities in the nucleus are still poorly understood. The presence of PPIns and their metabolizing enzymes in the nucleus emerged in the 1980´ when Smith and Wells showed that PPIns could be generated in the nuclear envelope by the presence of specific phosphoinositide kinases and phosphatases in rat liver (Smith and Wells, 1983, Smith and Wells, 1984). A few years later, in 1987, Cocco *et al*. showed that PPIns and their metabolizing enzymes also are present within the nucleus of murine erythroleukemia cells when the nuclear membrane was

stripped off (Cocco et al., 1987). It was also shown that the nuclear pools of PPIns are independently regulated from the cytosolic pool (Divecha et al., 1991, Cocco et al., 1989). Since then, it has been reported that nuclear PPIns are involved in several nuclear functions such as mRNA processing, chromatin remodelling, transcription, epigenetics and DNA repair (Castano et al., 2019).

All PPIns except for PtdIns(3,5)P_2 and their metabolizing enzymes have been detected and localized within the nucleus using different approaches such as radiolabelling, lipid binding affinity probes, or antibodies against specific PPIns or their metabolizing enzymes (Kalasova et al., 2016, Chen et al., 2020, Jacobsen et al., 2019). PPIns and their metabolizing enzymes have been localized to various nuclear sub-compartments such as the nuclear speckles and nucleoli as well as to the nucleoplasm, nuclear matrix, chromatin and the nuclear membrane (Jacobsen et al., 2019, Chen et al., 2020).

While the nucleus is a double-membrane organelle containing an inner and an outer membrane, the nuclear sub-compartments are membraneless (Mao et al., 2011). This raises the question of how the hydrophobic acyl chains of PPIns are protected from the aqueous environment of the nuclear compartment. It has been hypothesised that the hydrophobic acyl chains can be hidden in a hydrophobic pocket of a carrier protein, while the myo-inositol ring is exposed to the solvent (Barlow et al., 2010). Indeed, studies have shown that the nuclear receptors steroidogenic factor-1 (SF-1, *NR5A1*) and liver receptor homolog 1 (LRH-1, *NR5A2*) can bind PPIns (Krylova et al., 2005). Crystal structures of PtdIns(4,5)P_2 and PtdIns(3,4,5)P_3 bound to SF-1 and PtdIns(3,4,5)P_3 bound to LRH-1 show that the PPIns hydrophobic tails are hidden in the hydrophobic pocket of SF-1/LRH-1, while their headgroups are exposed to the solvent (Blind et al., 2014, Sablin et al., 2015). Blind *et al.* also demonstrated that PtdIns(4,5)P_2 and PtdIns(3,4,5)P_3 bound to SF-1 could be phosphorylated and dephosphorylated by inositol polyphosphate multikinase (IPMK) and the tumor suppressor phosphatase and tensin homolog (PTEN), respectively (Blind et al., 2012). Furthermore, Sobol *et al.* have described a new nuclear structure called Nuclear lipid islet (NLI), a globular structure that among others contains PtdIns(4,5)P_2 with its inositol headgroup directed outward and the hydrophobic acyl chains directed inwards (Sobol et al., 2018).

Identifying nuclear PPIn binding proteins helps to better understand their nuclear function, and to date, several PPIn binding proteins and their functional roles have been characterized. For

example, PtdIns5*P* binds to Arabidopsis homolog of trithorax 1 (ATX1) via the plant homeodomain (PHD) finger and this interaction has been shown to negatively regulate ATX1 and the expression of a set of genes (Alvarez-Venegas et al., 2006). Meanwhile, PtdIns(4,5)P_2 has been shown to interact and regulate the activity of the non-canonical poly(A)polymerase, STAR-PAP (Nuclear speckle targeted PIPKIα regulated-poly(A) polymerase) which is involved in regulating the expression of a set of nuclear mRNAs (Mellman et al., 2008). PtdIns(4,5)P_2 and PtdIns(3,4,5)P_3 interact directly with the mRNA export protein ALY, which is necessary for its localization to nuclear speckles (Okada et al., 2008). PtdIns(3,4,5)P_3 also interacts with the nucleolar phosphoprotein nucleophosmin (NPM)/ B23 in nerve growth factor (NGF) treated PC12 cells, where they mediate anti-apoptotic events of NGF by inhibiting caspase-activated DNase (CAD) (Ahn et al., 2005). Proteins such as SAP30 (Sin3A-associated protein 30), SAP30L (SAP30-Like) and pf1 (plant homeodomain zinc finger 1) are other examples of nuclear proteins that bind mono-phosphorylated PPIns via PBRs (Viiri et al., 2009, Kaadige and Ayer, 2006).

1.1.5 PtdIns(3,4,5)P_3 and the phosphoinositide-3- kinase (PI3K) pathway

PtdIns(3,4,5)P_3 or PIP_3 is the least abundant of the PPIns and it is barely detectable in quiescent cells (De Craene et al., 2017). Yet, PIP_3 is an important secondary messenger for many cellular processes such as cell proliferation, growth, survival and metabolism. Upon stimulation, the levels of PIP_3 can increase up to a 100-fold by the activity of phosphoinositide-3 kinases (PI3Ks) (De Craene et al., 2017).

PI3K is a family of enzymes that phosphorylates the 3′-hydroxyl group of PtdIns and its phosphorylated derivatives (Vanhaesebroeck et al., 2010). The PI3K family can be divided into three subclasses (I, II and III) based on lipid specificity and structure (Vanhaesebroeck et al., 2010). In vivo, PtdIns3*P* is generated from PtdIns (class II and III), while PtdIns(3,4)P_2 is generated from PtdIns4*P* (class II) and finally PIP_3 is generated from PtdIns(4,5)P_2 (class I) (Jean and Kiger, 2014). Class I PI3Ks are heterodimers and consist of a regulatory- and a catalytic subunit (Bilanges et al., 2019). The enzymes can further be divided into class IA and class IB based on their catalytic and regulatory components. Enzymes of class IA contains one of the three catalytic isoforms p110α, p110β or p110δ which can interact with one of the regulatory subunits p85α, p50α, p55α, p85β or p55γ. Meanwhile, class 1B consists of a p110γ catalytic subunit and a p84/p87 or p101 regulatory subunit (Bilanges et al., 2019) (Table

1.1). The expression of p110α and p110β is seen in most cell types, whereas p110δ and p110γ are predominantly expressed in leukocytes (Bilanges et al., 2019).

Table 1.1: Catalytic- and regulatory subunits of class I PI3K

Class I PI3K	Catalytic subunit (gene name)	Regulatory subunit (gene name)
Class IA	p110α (*PIK3CA*) p110β (*PIK3CB*) p110δ (*PIK3CD*)	p85α, p50α, p55α, (*PIK3R1*) p85β (*PIK3R2*) p55γ (*PIK3R3*)
Class IB	p110γ (*PIK3CG*)	p101 (*PIK3R5*) p84/p87 (*PIK3R6*)

Upon activation of either receptor tyrosine kinase (RTK) or G protein-coupled receptors (GPCRs), the class I PI3K gets activated and subsequently catalyse the formation of PIP_3 (Kriplani et al., 2015). PIP_3 can further recruit various effector proteins to the membrane, such as the serine/threonine kinase AKT (also known as protein kinase B, PKB), Phosphoinositide-dependent kinase-1 (PDK1) and Bruton's tyrosine kinase (BTK) (Kriplani et al., 2015). All of these proteins contain a PH-domain that binds to PIP_3 (Kriplani et al., 2015). The activation of the effector proteins further leads to the activation of many downstream signalling pathways (Kriplani et al., 2015).

PIP_3 is an important secondary messenger for many cellular processes and it is tightly regulated. PTEN is a negative regulator of PIP_3 and act by dephosphorylating the 3´hydroxyl group of PIP_3 to generate PtdIns(4,5)P_2 (Maehama and Dixon, 1998). PTEN is a tumor suppressor protein and mutations of PTEN are implicated in several diseases including cancer (Chalhoub and Baker, 2009). Another regulator of PIP_3 is the Src homology 2 (SH2) domain-containing inositol 5´phosphatase (SHIP) 1 and 2, which dephosphorylate the 5´hydroxyl group of PIP_3 to generate P(3,4)P_2 (Damen et al., 1996, Backers et al., 2003).

PIP_3 and PI3K in the nucleus

Studies have demonstrated that members of the PI3K pathway including PtdIns(4,5)P_2 and PIP_3 as well as the kinases and phosphatases that metabolize them are present within the nucleus at various sub-nuclear structures, where they have distinct nuclear functions (Jacobsen et al., 2019). PtdIns(4,5)P_2, the precursor of PIP_3 has been located to nuclear speckles and in lesser extent to the nucleolus by immunofluorescence staining (Boronenkov et al., 1998, Yildirim et

al., 2013, Kalasova et al., 2016). Meanwhile, PIP_3 has been localized to the nuclear matrix and the nucleolus using either a GST-GRP1-PH probe (specifically binds PIP_3), or specific anti-PIP_3 antibodies (Lindsay et al., 2006, Karlsson et al., 2016, Gavgani et al., 2019). In the nucleus, PIP_3 has been shown to be generated by at least two enzymes including class I PI3K p110β and IPMK that both uses PtdIns(4,5)P_2 as a substrate (Kumar et al., 2010, Resnick et al., 2005). P110β contains an NLS in its C2 domain, and when in complex with p85β regulatory subunit which contains a nuclear export signal (NES), it can shuttle between the cytoplasm and nucleus (Kumar et al., 2011). P110β has also been implicated in various nuclear functions such as DNA replication, DNA double strand break repair (DSBR) and cell survival (Marqués et al., 2009, Kumar et al., 2010, Kumar et al., 2011). Moreover, the phosphatases PTEN and SHIP 1/2, which are all known to antagonize PIP_3 have been detected within the nucleus as well (Déléris et al., 2003, Nalaskowski et al., 2012).

Characterizing the function of PIP_3 and its nuclear binding proteins can contribute to a better understanding of its nuclear roles. However, only a few nuclear PIP_3 binding proteins have been identified so far. PIP_3 binds to proteins such as ALY and NPM as previously mentioned(Okada et al., 2008, Ahn et al., 2005). Moreover, PIP_3 binds to the PtdIns(3,4,5)P_3 binding protein (PIP_3-BP) via two PH-domains in brains (Tanaka et al., 1997, Tanaka et al., 1999). The PI3K enhancer (PIKE)-L is another PH domain containing protein that binds to PIP_3 in the nucleus (Hu et al., 2005). In addition, PIP_3 binds to ErbB3-binding protein 1 (EBP1) via a polybasic motif in the nucleolus (Karlsson et al., 2016).

PI3K in the nucleolus

Nucleolar structure

The nucleolus is one of the largest, membraneless subnuclear structures in the nucleus (Mao et al., 2011). Its main role is ribosome biogenesis, which includes transcription and processing of ribosomal RNA (rRNA), assembly of ribosomes, and transport of the ribosomes to the cytoplasm (Tiku and Antebi, 2018) (Figure 1.3A). The nucleolus is a dynamic structure and it is regulated during the cell cycle, where it disassembles and assembles when the cell enters and exits mitosis, respectively (Tiku and Antebi, 2018). The nucleolus is formed around the nucleolar organizing regions (NORs), which consists mainly of tandemly repeated ribosomal genes (rDNA) located on the short arms of human acrocentric chromosomes (13, 14, 15, 21, 22) that encode for 18S, 5.8S and 28S rRNAs (Farley et al., 2015, McStay, 2016). The rDNA

is first transcribed into a 47S precursor rRNA by RNA polymerase I, which is then processed and modified to generate the 18S, 5.8S and 28S rRNAs (Farley et al., 2015). 5S rRNA is transcribed by RNA polymerase III outside the nucleolus and is transported into the nucleolus along with ribosomal proteins (transcribed by RNA polymerase II) to assemble the 40S and 60S ribosomal subunits (Pelletier et al., 2018). These subunits are subsequently transported to the cytoplasm where they form the mature 80S ribosome which can then start the translation of mRNAs into proteins (Pelletier et al., 2018).

Structurally, the mammalian nucleoli are divided into three subregions that can be observed in an electron microscope (Sirri et al., 2008). These include the fibrillar centre (FC), the dense fibrillar component (DFC), and the granular component (GC), in which the different steps of the ribosome biogenesis takes place (Sirri et al., 2008) (Figure 1.3A). The transcription of pre-rRNA occurs at the boundary between the FC and DFC, while the pre-rRNA processing occurs at the DFC. Finally, the assembly of pre-ribosomal subunits happens at the GC before they are transported out to the cytoplasm (McStay, 2016). Furthermore, the nucleolus is surrounded by a condensed heterochromatin shell that among others contains silent rDNA (Guetg and Santoro, 2012, Schöfer and Weipoltshammer, 2018). A subnuclear compartment called the perinucleolar compartment (PNC) is associated on the periphery of the nucleolus. The function of the PNC is not known; however, it is enriched in RNA binding proteins and RNA polymerase III transcribed RNAs (Pollock and Huang, 2010). The PNC is mostly observed in cancer cells and rarely seen in normal cells (Wen et al., 2013).

Even though ribosome biogenesis is the main function of nucleoli, proteomic studies have identified over 4500 proteins to associate with the nucleolus, in which several of them have other roles than in the synthesis of ribosomes (Ahmad et al., 2009). The nucleolus has been implicated in various roles such as cell cycle progression, biogenesis of ribonucleoproteins (RNPs), stress response, genome integrity maintenance, epigenetic control and cellular senescence (Boisvert et al., 2007, Tiku and Antebi, 2018, Lindström et al., 2018).

PI3K in the nucleolus

The PI3K signalling pathway has been implicated to have various roles in ribosome biogenesis. Several components of the pathway have been localized to the nucleoli over the past years, including PtdIns(4,5)P_2 (Sobol et al., 2013, Yildirim et al., 2013), the class I PI3K isoform p110β and its product, PIP_3 (Karlsson et al., 2016, Gavgani et al., 2019), as well as the two

phosphatases PTEN and SHIP-1(Li et al., 2014, Ehm et al., 2015) (Figure 1.3B). For example, using *Drosophila* S2R+ cells it was shown that inhibition of PI3K or mTOR with LY294002 and rapamycin, respectively, resulted in decrease of rRNA synthesis (Vinayagam et al., 2016). Moreover, AKT was shown to mediate an increase in rRNA synthesis by activating the transcription initiation factor I (TIF-IA) which is required for rDNA transcription (Nguyen and Mitchell, 2013). In addition, it has been shown that activation of PI3K through Insulin receptor substrate I (IRS-I) leads to phosphorylation and activation of the nucleolar transcription factor UBF-1 (Upstream binding factor-1), by the PI3K p110 subunit, which is likely to be the p110β isoform due to its presence in the nucleolus (Drakas et al., 2004, Gavgani et al., 2019). A nuclear PIP_3 interactome study by our group revealed that among the 179 nuclear proteins that were identified to be in complex with PIP_3, 29-40% of them were annotated to the nucleolus, indicating that PIP_3 might regulate several functions in this nuclear structure. PARP-1 was one of the proteins that was identified as a potential PIP_3 binding partner, and our group decided to further investigate their interaction due to the reported nucleolar localization of PARP-1 (Mazloumi Gavgani et al., 2017) (see section 1.2.5).

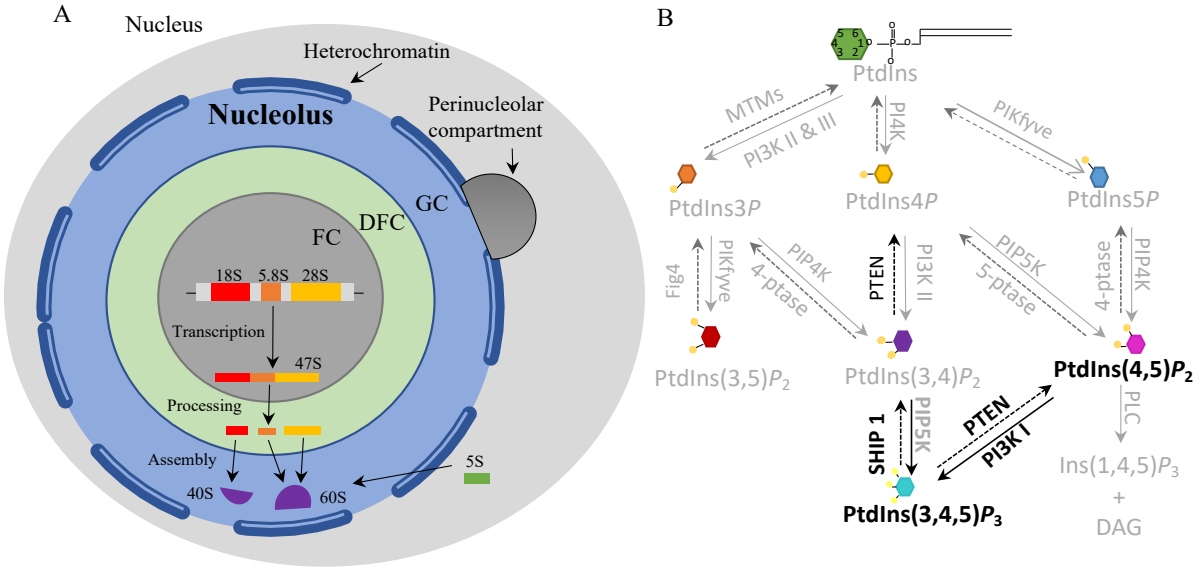

Figure 1.3: The PI3K pathway in the nucleolus. A) Structural and functional overview of the nucleolus and ribosome biogenesis. The nucleolus can be divided into three subregions including the fibrillar center (FC), the dense fibrillar component (DFC) and the granular component (GC). The nucleolus is also surrounded by a perinucleolar heterochromatin shell and a perinucleolar compartment is associated on the periphery of the nucleolus. During ribosome biogenesis, the ribosomal DNA (rDNA) is transcribed into a 47S precursor ribosomal RNA (rRNA) by RNA polymerase I. The pre-rRNA is further processed to generate the 18S, 5.8S and 28S rRNAs. 5S rRNA is further transported into the nucleolus to mediate the assembly of the 40S and 60S ribosomal subunits. **B)** Components of the PI3K signaling pathway which have been detected within the nucleolus (highlighted in black). Abbreviations: SHIP-1: the Src homology 2 (SH2) domain-containing inositol 5′phosphatase PTEN: phosphatase and tensin homolog, PI3K 1: class 1 phosphoinositide 3-kinase.

1.2 Poly(ADP-ribose) Polymerase 1 (PARP-1)

1.2.1 PARP-1 and the PARP family

ADP ribosylation is a post-translational modification catalysed by a family of enzymes called poly(ADP-ribose) polymerases (PARPs, also known as ADP-ribosyl transferase diphtheria toxin-like; ARTD) (Hottiger et al., 2010). The PARP superfamily consists of 17 distinct enzymes that all share a conserved catalytic domain, the ADP-ribosyltransferase (ART) domain. Beside of the catalytic domain, the enzymes vary in structure and function and are located to different cellular compartments (Gupte et al., 2017). Based on the structure and function, the PARP superfamily can be divided into four subfamilies including the DNA dependent PARPs (PARP 1-3), tankyrases (PARP 5a and b), CCCH (Cys-Cys-Cys-His) zinc finger PARPs (PARP 7/12/13) and macro PARPs (PARP 9/14/15). The rest of the PARP family members have been referred to as unclassified PARPs (Vyas et al., 2013). PARPs act by covalently attaching mono- or poly(ADP-ribose) (MAR or PAR) on target proteins using nicotinamide adenine dinucleotide (NAD+) as a substrate (Gupte et al., 2017). The ADP-ribose polymers can be linear or branched and up to 200 units long (D'Amours et al., 1999). Proteins can also bind non-covalently to PAR and in that manner have their function regulated or be recruited to a specific site (Krishnakumar and Kraus, 2010). Several domains or motifs that bind MAR or PAR have been discovered and include among others the macrodomains, the PAR binding zinc finger (PBZ) domains and the PAR binding motifs (PBM) (Gupte et al., 2017, Barkauskaite et al., 2013). The PARP family of enzymes regulate several cellular processes such as chromatin remodelling, transcription, DNA repair, apoptosis and various cytoplasmic stress responses (Gupte et al., 2017, Bock and Chang, 2016). Their activities are tightly regulated, and PAR is rapidly degraded by a set of proteins such as Poly(ADP-ribose) glycohydrolase (PARG) and ADP-ribosylhydrolase(ARH) 3, while MacroD1, MacroD2, Terminal ADP-Ribose protein Glycohydrolase (TARG1) and ARH 1 remove MAR (Slade et al., 2011, Mueller-Dieckmann et al., 2006, Rosenthal et al., 2013).

Poly(ADP-ribose) polymerase 1 (PARP-1) is the founding member of the PARP family and is also the most studied. PARP-1 is an abundant nuclear enzyme found in eukaryotic organisms (Jubin et al., 2016). The enzyme has been shown to be involved in several functions including chromatin remodelling, DNA repair, replication and transcription, and act by post-translationally modifying itself as well as other target proteins by PARylation (Jubin et al., 2016). Moreover, PARP-1 is responsible for 80-90% of the total cellular PARylation (Jubin et

al., 2016) and is also a therapeutic target in several cancers due to its nuclear enzymatic activity (Rouleau et al., 2010).

1.2.2 PARP-1 structure

Human PARP-1 is a 113 kDa protein (1014 aa) consisting of an N-terminal DNA binding domain (DBD, aa 1- 374), a central auto-modification domain (AD, aa 375-525) and a C-terminal catalytic domain (aa 526-1040) (Langelier et al., 2008) (Figure 1.4).

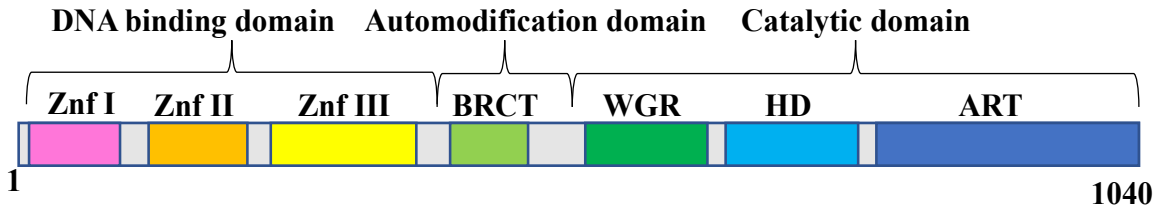

Figure 1.4: Schematic representation of human PARP-1 structural and functional domains. PARP-1 is a multidomain protein with three main domains. PARP-1 has a DNA binding domain which contains three zinc finger motifs (Znf I-III), an automodification domain (AD) which contains a BRCA1 C-terminal domain (BRCT) and a catalytic domain which contains a Trp-Gly-Arg (WGR) domain, a Helical subdomain (HD) and an (ADP-ribosyl) transferase domain (ART).

Three zinc finger motifs (ZnF I-III), a bipartite nuclear localization signal (NLS, 207-226) and a caspase-3 cleavage site (^{211}DEVD^{214}) are found within the DBD of PARP-1 (Langelier et al., 2008, Schreiber et al., 1992, Soldani and Scovassi, 2002). The homologous ZnF-I and ZnF-II are important for the recognition and binding of PARP-1 to DNA structures such as single- and double-strand breaks (SSB and DSB) which further leads to the activation of the catalytic domain of PARP-1 (Langelier et al., 2011). ZnF-III differs from the two other zinc fingers in both structure and function and is involved in DNA binding as well as in the enzymatic activation of PARP-1 via an inter-domain interaction between the DNA binding region and the catalytic domain (Langelier et al., 2008, Langelier et al., 2012).

The AD contains a BRCA1 C-terminal domain (BRCT) which is involved in protein-protein interactions and is essential for interactions with proteins such as X-ray repair cross-complementing protein 1 (XRCC1) involved in DNA repair (Maluchenko et al., 2015). The AD is also the site of PAR auto-modification and at least three lysine residues (Lys-498, 521 and 524) have been shown to be targeted. (Altmeyer et al., 2009).

The catalytic domain contains a tryptophan- glycine- arginine (WGR) domain, a helical subdomain (HD) and an (ADP-ribosyl) transferase domain (ART). The WGR domain is named

after its conserved Trp-Gly-Arg motif and is involved in DNA binding and interdomain interactions (Langelier et al., 2012). The HD domain acts as an inhibitor by blocking the binding of NAD^+ to the active site of PARP-1. Binding of PARP-1 to damaged DNA leads to a conformational change and a local unfolding of the HD which makes the active site available for NAD^+ (Dawicki-McKenna et al., 2015). The ART domain is conserved in the PARP superfamily and includes the active site for binding of NAD^+ (Alemasova and Lavrik, 2019). PARP-1 perform three catalytic activities which includes 1) the initial addition of an ADP-ribose moiety to an acceptor amino acid 2) elongation by additional attachment of ADP-ribose moieties and 3) branching of ADP-ribose polymers (Alemasova and Lavrik, 2019). In the absence of DNA, each independent domain is linked to each other by a flexible linker like "beads on a string" (Alemasova and Lavrik, 2019).

1.2.3 PARP-1 and DNA repair

Organisms are prone to various DNA damages caused by either endogenous metabolic processes such as hydrolysis, oxidation, alkylation, mismatch of DNA bases, or by exogenous agents such as ionizing radiation (IR), UV-radiation or chemicals (Hakem, 2008). If the DNA damage is not properly repaired, it can lead to mutations and the development of diseases such as cancer, as well as senescence or apoptosis (Hakem, 2008). To maintain the genomic integrity, cells have developed several DNA repair mechanisms (Hakem, 2008). PARP-1 has important roles in response to DNA damage such as repair of single- and double strand breaks (SSB and DSB), regulation of chromatin structure and in stabilizing the DNA replication fork. (Ray Chaudhuri and Nussenzweig, 2017).

Upon DNA damage, PARP-1 will rapidly recognize and bind to SSB or DSB and subsequently catalyse the formation of PAR both on itself and other target proteins such as chromatin remodelling- and DNA repair factors (Ray Chaudhuri and Nussenzweig, 2017). The binding of PARP-1 to damaged DNA increases PAR-activity up to 500-fold (D'Amours et al., 1999). However, long negatively charged polymers will eventually cause PARP-1 to be released from the DNA due to repulsion, and the PAR polymers are rapidly degraded by PARG within a few minutes (Luo and Kraus, 2012). Several studies have demonstrated the involvement of PARP-1 in multiple DNA repair pathways including nucleotide excision repair (NER), base excision repair (BER), single-strand break repair (SSBR), mismatch repair (MMR), non-homologous end joining (NHEJ) and homologous recombination (HR) (Ko and Ren, 2012) In addition,

PARP-1 mediates the relaxation of chromatin structures to make the damaged DNA more accessible for DNA repair factors. PARP-1 does so by PARylating histones and by recruiting chromatin remodelling factors such as Amplified in liver cancer 1 (ALC1) (Ray Chaudhuri and Nussenzweig, 2017).

SSB is one of the most frequent type of DNA damage in cells and can results from either free radicals such as reactive oxygen species (ROS, e.g. H_2O_2) or indirectly from the BER pathway (Caldecott, 2008). PARP-1 recognizes the damaged DNA in an early stage of the BER/SSBR pathway and quickly PARylates itself as well as other molecules (Caldecott, 2008). XRCC1 interacts directly with PARP-1 in a PAR-dependent manner and is immediately recruited to the damaged site. XRCC1 acts as a scaffold protein and further recruit and stimulate the enzymatic activity of other SSBR factors (Caldecott, 2008). PARP-1 interacts with other BER/SSBR factors such as DNA ligase III, DNA polymerase β and proliferating cell nuclear antigen (PCNA) as well (Wei and Yu, 2016). In addition, PARP-2 has been shown to mediate BER/SSBR and interacts with proteins such as XRCC1, DNA ligase III and DNA polymerase β (Schreiber et al., 2002).

DSB is a more severe type of DNA damage that can be induced endogenously from ROS and collapsed replication forks or by exogenous sources such as IR or chemicals (Beck et al., 2014). PARP-1 mediates DSBR via two major repair pathways; HR, which is an error-free pathway that uses sister chromatid as a template, and NHEJ, which re-joins the damaged DNA strands directly to each other (Beck et al., 2014). For example, PARP-1 recruits ataxia telangiectasia mutated (ATM) and meiotic recombination 11 (Mre11) in a PAR-dependent manner to the DNA damaged site (Ray Chaudhuri and Nussenzweig, 2017). Mre11 is part of the Mre11-RAD50-NBS1 (WRN) complex involved in HR. PARP-1 is also involved in the recruitment of breast cancer type 1 susceptibility protein (BRCA-1) which is another important factor in HR (Ray Chaudhuri and Nussenzweig, 2017). PARP-1 has been implicated in the classical NHEJ by PARylating and stimulating the activity of DNA-dependent protein kinase catalytic subunit (DNA-PKcs) (Ray Chaudhuri and Nussenzweig, 2017). In the absence of the classical NHEJ, the cell can promote an alternative NHEJ (alt-NHEJ) repair pathway. PARP-1 contributes in this pathway by recruiting DNA repair factors such as XRCC1 and Polynucleotide Kinase 3'-Phosphatase (PNKP) (Wei and Yu, 2016). Additionally, PARP-2 and PARP-3 have also been implicated in DSBR (Beck et al., 2014).

PARP-1 mediates DNA repair and cell survival in response to mild DNA damages. However, if the DNA damage is too extensive, PARP-1 will instead promote cell death. PARP-1 is involved in several cell death pathways, including necrosis, apoptosis and parthanatos (Koh et al., 2005). Extensive DNA damage promotes hyperactivation of PARP-1 and PAR-production, which can lead to NAD^+ depletion and subsequently ATP deficiency. Prolonged deficiency of NAD+ and ATP causes the cell to go through necrosis (Koh et al., 2005). Apoptosis, which inactivates PARP-1 can however prevent the cell from a necrotic cell death (Soldani and Scovassi, 2002). PARP-1 can be cleaved into a DBD fragment (24 kDa) and a catalytic fragment (89 kDa) by capsase-3 and caspase-7 (Soldani and Scovassi, 2002). Inhibition of PARP-1 subsequently prevents the cell from ATP depletion which is required for the apoptotic pathway (Soldani and Scovassi, 2002). The last pathway, Parthanatos, is a PARP-1 dependent cell death pathway (Fatokun et al., 2014). PARP-1 hyperactivation and PAR-polymer formation can lead to signalling and translocation of apoptosis-inducing factor (AIF) from mitochondria to the nucleus. In the nucleus, AIF mediates cell death by contributing to a large-scale DNA fragmentation and chromatin condensation (Fatokun et al., 2014).

1.2.4 PARP-1 in the nucleolus

Several studies have demonstrated that PARP-1 accumulates in the nucleolus and more specifically within the DFC (Fakan et al., 1988, Mosgoeller et al., 1996). However, the exact roles of PARP-1 in the nucleolus are still largely unknown. So far, PARP-1 has been shown to interact with several nucleolar proteins including NPM/B23, Fibrillarin and Nucleolin (Meder et al., 2005, Boamah et al., 2012). Moreover, the nucleolar localization of PARP-1 is dependent upon active transcription of RNA by RNA polymerase I (Meder et al., 2005). In *Drosophila,* PARP-1 and its enzymatic activity have been shown to be important for the structural integrity of the nucleoli and for the localisation of nucleolar-specific proteins such as Fibrillarin, and AJ1 in proximity of precursor RNA (Boamah et al., 2012) Loss of PARP-1 in *Drosophila* leads to fragmentation of the nucleolus and de-localisation of several nucleolar proteins important for ribosome biogenesis (Boamah et al., 2012). Moreover, inhibition of PARP-1 activity leads to an increase in rRNA intermediates and reduced levels of ribosomes, indicating that PARP-1 is involved in the synthesis of ribosomes (Boamah et al., 2012). Guetg *et al*. has shown that nucleolar PARP-1 and its enzymatic activity mediate the transcriptional silencing of rRNA genes and in silent rDNA chromatin formation by interactions with TIP5 (TTF-1-interacting protein 5) a component of the nucleolar remodelling complex (NoRC) via noncoding pRNA

(Guetg et al., 2012). Furthermore, PARP-1 has been shown to bind small nucleolar RNA (snoRNA) which leads to the PARylation of the DEAD-box RNA helicase DDX21 (Kim et al., 2019). When PARylated, DDX21 interacts with rDNA chromatin and increases rDNA transcription and cell growth in breast cancer cells (Kim et al., 2019). Additionally, PARP-1 mediates the nucleolar-nucleoplasmic shuttling of the DNA repair factors, WRN and XRCC1 upon DNA damage (Veith et al., 2019).

1.3 Aims of the study

The PI3K pathway is important for many cellular processes and beside of being localized to the plasma membrane, several studies have shown that members of the PI3K pathway are found within the nucleus, where they have been shown to mediate several nuclear functions (Jacobsen et al., 2019). P110β and its product, PIP_3, have been localized to the nucleoplasm and the nucleolus (Karlsson et al., 2016, Gavgani et al., 2019). However, the functional role of PIP_3 is still largely unknown as only a few nuclear effector proteins have been characterized so far. Previously, the nuclear PIP_3 interactome was mapped using nuclear extract from HeLa cells and PARP-1 was among others identified as a potential PIP_3 binding partner (Mazloumi Gavgani et al., 2017). This binding was further confirmed by *in vitro* lipid overlay assay, where recombinant GST-PARP-1 bound to several PPIns, including PIP_3. Moreover, it was shown that PARP-1 and PIP_3 co-localizes in the nucleolus in HeLa cells (Mazloumi Gavgani et al., 2017). PARP-1 is a highly abundant nuclear protein involved in several nuclear functions such as DNA repair, transcription, and chromatin remodelling (Jubin et al., 2016). PARP-1 does not contain any specific PPIn-binding domains; however, it does contain several PBR/K/R motifs which are known to bind PPIns. The present study aimed to look further into the interaction between PARP-1 and PIP_3. In particular, this study aimed to:

1. Determine the PIP_3 interaction sites of PARP-1 by generating mutants using recombinant GST-PARP-1 fragments and assess their binding affinities for various lipids including the seven PPIns using lipid overlay assay.

2. Determine whether PIP_3 is important for the regulation of PARP-1 enzymatic activity upon H_2O_2 induced DNA damage using MEF cells harbouring WT or kinase dead versions of the class I PI3K isoform p110β.

2 Materials

Table 2.1.1: Chemicals

Chemicals	Grade/ purity	Abbrev. Formula	Supplier	Cat. No.
2-amino-2-hydroxymethyl-1,3-propanediol, Trizma® base	ANG	Tris	Sigma-Aldrich®	T6066
30 % Acrylamide/Bis-acrylamide			Sigma- Aldrich®	A3699
4-(1,1,3,3-Tetramethylbutyl) phenyl-polyethylene glycol	MBG	Triton® X-100	Sigma-Aldrich®	T8787
Acetic acid	100 %	CH_3OOH	VWR Chemicals	20104.367
Agarose			Sigma- Aldrich®	A9539
Ammonium persulfate		APS	Bio-Rad	161-0700
Ampicillin		Amp	Sigma-Aldrich®	A9393
Bovine serum albumin, essentially fatty acid free	≥96 %	BSA FF-free	Sigma- Aldrich®	A6003
Dimethyl Sulfoxide		DMSO	Sigma-Aldrich®	472301
DL-Dithiothreitol		DTT	Sigma-Aldrich®	D9163
Ethanol	100 %	EtOH	VWR Chemicals	20821.330
Ethidium Bromide		EtBr	Sigma-Aldrich®	E1510
Hydrogen peroxide solution	≥ 30 %	H_2O_2	Sigma-Aldrich®	95321
IGEPAL® CA-630		IGEPAL	Sigma-Aldrich®	I8896
Isopropanol		IPA	Kemetyl	600079
Isopropyl ß-D-1-thiogalactopyranoside		IPTG	Apollo Scientific	BIMB1008
Kanamycin sulfate		Kan	Sigma-Aldrich®	K4000
L-glutathione, reduced form	≥ 98 %		Sigma-Aldrich®	G4251
lysogeny broth		LB	Sigma- Aldrich®	L3022
LB-Agar	MBG		Sigma-Aldrich®	L2897
Methanol	≥ 99.8 %	MeOH	Sigma-Aldrich®	32213
N,N,N',N'-tetramethylethylenediamine		TEMED	Bio-Rad	161-0800
Non-fat milk powder			Sainsbury´s	
Paraformaldehyde		PFA	Merck	K40988605
Polyoxyethylenesorbitan monolaurate		TWEEN®-20	Sigma-Aldrich®	P1379
Potassium chloride	ANG	KCl	Merck	1.04936

Sodium chloride	≥99.8 %	NaCl	Sigma-Aldrich®	31434N
Sodium dihydrogen phosphate		NaH2PO4·H2O	Merck	1.60346
Titriplex® ethylenedinitrilotetraacetic acid disodium salt dehydrate	ANG	EDTA	Merck	1.08418

ANG=Analyse grade MBG=Molecular biology grade

Table 2.1.2: Commercial kits and reagents

Name	Supplier	Application
BigDye v.3.1	Thermo Fisher Scientific	DNA sequencing
Gel Loading Dye, Purple (6X)	New England BioLabs Inc.	Agarose gel electrophoresis
Glutathione Sepharose® 4B	GE healthcare Life Sciences	Purification of GST-tagged recombinant proteins
Goat serum	Thermo Fisher Scientific	Blocking
InstantBlue™ Protein stain	Expedon	Coomassie protein stain
NucleoBond® Xtra Midi	Macherey-Nagel	Midi prep
NucleoSpin® Plasmid	Macherey-Nagel	Mini prep
PIP strips™	Echelon Biosciences Inc.	Lipid overlay assay
ProLong® Glass antifade mountant with NucBlue	Thermo Fisher Scientific	Cell slide mounting
Sequencing buffer	Thermo Fisher Scientific	DNA sequencing
S.O.C medium	Thermo Fisher Scientific	Transformation
SuperSignal™ West Pico Plus Chemiluminescent Substrate	Thermo Fisher Scientific	Lipid blot visualization
QuickChange II Site-Directed Mutagenesis Kit	Agilent	Site directed mutagenesis

Table 2.1.3: Ladders

Ladder	Supplier	Application	Cat. No.
2-log DNA ladder (0.1-10.0 kb)	New England BioLabs Inc.	Agarose gel electrophorese	N3200S
Precision Plus Protein™ standard	BIO-RAD	SDS-PAGE	161-0374

Table 2.1.4: Instruments

Equipment	Supplier	Application
Allegra® X-15R Centrifuge	Beckman Coulter	Centrifugation
Avanti® J-26 XP Centrifuge	Beckman Coulter	Centrifugation
ChemiDoc XRS+™	Bio-Rad	Lipid blot imaging
Fluorescence microscope DMI 6000 B	Leica Microsystems	Fluorescent imaging
GelDoc EZ Imager	Bio-Rad	SDS-PAGE and agarose gel
GenAmp® PCR System 2700	Applied Biosystems	PCR
NanoDrop ND-1000™ Spectrophotometer	Saveen Werner	DNA and protein concentration

Table 2.1.5: Software

Name	Purpose	Developer
Fiji (v. 2.0.0)	Cell image analysis	Schindelin et al. (2012)
Image Lab	Agarose gel, SDS-PAGE and lipid blot imaging	Bio-Rad
Leica Application suite Advanced Fluorescence (LAS AF)	Cell imaging	Leica Microsystems
PyMOL (v. 2.3.0)	Visualization of protein structure	Schrödinger LLC
MUSCLE	Multiple sequence alignment	Edgar (2004)
ApE- a plasmid editor (v. 2.0)	Aligning sequences	M. Wayne Davis

Table 2.1.6: Cell culture reagents

Reagent	Supplier	Cat. No.
Dulbecco's Modified Eagle's Medium (DMEM) - high glucose (With 4500 mg/L glucose and L-glu)	Sigma-Aldrich®	D6429
Fetal bovine serum (FBS)	Sigma-Aldrich®	F7524
100x Penicillin-Streptomycin (PEN/STREP)	Merck	TMS-AB2-C
Trypsin-EDTA	Sigma-Aldrich®	T4049

Table 2.1.7: Cell lines

Cell line	Description	Supplier
HeLa WT	Human cervix epithelioid carcinoma	M. Bakke, ATCC
MEF p110β WT	Mouse embryonic fibroblast p110β wild type	Dr Julie Guillermet-Guibert, University of Toulouse, France
MEF p110β KI (D931A/D931A)	Mouse embryonic fibroblast kinase dead version of the PI3K isoform p110β.	Dr Julie Guillermet-Guibert, University of Toulouse, France

Table 2.1.8: Primary antibodies

Name	Species	Supplier	Dilution (Application)	Cat. No
Fibrillarin	Rabbit	Cell signalling technology	1:100 (IF)	2639S
Nucleophosmin	Mouse	Thermo Fisher Scientific	1:500 (IF)	32-5200
PARP-1	Rabbit	Cell signalling Technology	1:60 (IF)	9542S
PAR (H10)	Mouse	Gift by Marc Niere	1:1000 (IF)	
PtdIns(4,5)P_2	Mouse	Thermo Fisher Scientific	1:200 (IF)	MA3-500

IF= Immunofluorescence

Table 2.1.9: Secondary antibodies

Name	Supplier	Dilution (Application)	Cat. No.
Goat anti-Rabbit Alexa Fluor 594	Thermo Fisher Scientific	1:200 (IF)	A-11012
Goat anti-Rabbit Alexa Fluor 488	Thermo Fisher Scientific	1:200 (IF)	A-11008
Goat anti-Mouse IgG Alexa fluor 594	Thermo Fisher Scientific	1:200 (IF)	A-11005
Goat anti-Mouse IgG Alexa fluor 488	Thermo Fisher Scientific	1:200 (IF)	A-11001
Goat anti-Mouse IgM Alexa fluor 594	Thermo Fisher Scientific	1:200 (IF)	A-21044
GST-HRP	Abcam	1:30 000 (LOA)	Ab3416

IF= Immunofluorescence LOA=Lipid overlay assay

Table 2.1.10: Bacterial strains

Bacterial strain	Supplier	Application
Escherichia coli XL1-Blue Supercompetent Cells	Agilent	Mutagenesis and plasmid purification
Escherichia coli BL21-CodonPlus(DE3) - RIL Competent Cells	Agilent	Protein expression

Table 2.1.11: Plasmids

Plasmid	Protein name	Amino acids	Restriction site
pGEX-6P-2	PARP-1 fragment 1	1-214 + His_6-tag	BamHI / NotI
pGEX-6P-2	PARP-1 fragment 2	215-371 + His_6-tag	BamHI / NotI
pGEX-6P-2	PARP-1 fragment 3	372-476 + His_6-tag	BamHI / NotI
pGEX-6P-2	PARP-1 fragment 4	477-524 + His_6-tag	BamHI / NotI
pGEX-6P-2	PARP-1 fragment 5	525-656 + His_6-tag	Xhol / Notl
pGEX-6P-2	PARP-1 fragment 6	657-1014 + His_6-tag	Xhol / Notl
pEGFP-C3	hPARP WT	1-1014	Pstl

*pGEX-6P-2 PARP-1 DNA fragments 1-6 were received from Prof. Michael O. Hottiger, University of Zurich, Switzerland
**The amino acid sequences of the PARP-1 fragments can be found in the Appendix.

Table 2.1.12: Primers used for site directed mutagenesis

Primers	Sequences 5´→ 3´
K84A K85L K87L FWD	GATGACCAGCAGGCAGTCTTGTTGACAGCGGAAGC
K84A K86L K87L REV	GCTTCCGCTGTCAACAAGACTGCCTGCTGGTCATC
Δ221-236 FWD	GTGGATGAAGTGGCGGCCCTAAAGGCTCAGAACG
Δ221-236 REV	CTGAGCCTTTAGGGCCGCCACTTCATCCACTCC
Δ346-352 FWD	GAAATCTCTTACCTCCAGGACCGTATATTCCCC
Δ346-352 REV	GAATATACGGTCCTGGAGGTAAGAGATTTCTCGG
K505A K506A FWD	GGCTGCGCTCTCCGCAGCAAGCAAGGGCCAGGTC
K505A K506A REV	CCTTGACCTGGCCCTTGCTTGCTGCGGAGAGCGCA
K508L FWD	CTCTCCGCAGCAAGCTTGGGCCAGGTC
K508L REV	GACCTGGCCAAGCTTGCCTGCGGAGAG
K505A K506A K508L FWD	TGCGCTCTCCGCAGCAAGCTTGGGCCAGGTC
K505A K506A K508L REV	GACCTGGCCCAAGCTTGCTGCGGAGAGCGCA

2.2 Buffers and solutions

2.2.1 Bacterial culture

LB-medium	LB-agar
1% (w/v) Tryptone	1.5 % (w/v) agar in LB-medium
1% (w/v) NaCl	
0.5% (w/v) yeast extract	

2.2.2 Agarose gel electrophoresis

1x TAE buffer	6x DNA sample buffer
40 mM Tris	30% Glycerol
20 mM Acetic acid	0.025% Bromophenol Blue
1 mM EDTA pH 8.0	

2.2.3 SDS-PAGE

Resolving gel	Stacking gel
12-13% of 30% Acrylamide/Bisacrylamide (37:5:1)	5% of 30% Acrylamide/Bisacrylamide (37:5:1)
375 mM Tris-HCl pH 8.8	125 mM Tris-HCl pH 6.8
0.1 % (v/v) SDS	0.1 % (v/v) SDS
0.1 % (v/v) APS	0.1 % (v/v) APS
0.04 % TEMED	0.04 % TEMED

5x SDS sample buffer

65 mM Tris-HCl pH 6.8

5% (v/v) SDS

20% (v/v) Glycerol

250 mM DTT

0.2 % (w/v) Bromophenol Blue

1x TGS running buffer

25 mM Tris pH 8.3

192 mM Glycine

0.1 % (w/v) SDS

2.2.4 Lipid overlay assay

1x TBS-T

150 mM NaCl

50 mM Tris pH 7.5

0.1% (v/v) Tween 20

Blocking buffer

3% (w/v) essentially fatty acid free BSA in TBS-T

2.2.5 Immunostaining

1x PBS pH 7.4

137 mM NaCl

2.68 mM KCl

8 mM $NaH_2PO_4 \cdot H_20$

1x PBS-T

0.05% (v/v) Tween 20 in 1x PBS

3 Methods

3.1 Site-directed mutagenesis

Three PARP-1 fragments (F1(1-214), F2 (215-371), F4 (477-524)) cloned into pGEX-6p-2, and the full length human PARP-1 (1-1014) cloned into pEGFP-C3 were used to generate four PARP-1 mutants, including fragment 1 K84A-K86L-K87L, fragment 2 Δ221-236, fragment 2 Δ346-352 and fragment 4 K505A-K506A-K508L (see Appendix for sequences). The mutants were generated using QuickChange II Site-Directed Mutagenesis Kit. The reaction consisted of 10 ng purified plasmid DNA as template, 0.2 or 0.25 µM of each primer (Table 2.1.12), 1x cloned Pfu reaction buffer, 1 µl dNTP mix, 3% DMSO and ddH_2O to a final volume of 50 µl followed by the addition of 2.5 U Pfu Turbo DNA polymerase. The PCR cycles were run with an initial denaturation at 95 ℃ for 30 sec followed by 20-22 cycles with denaturation at 95 ℃ for 30 sec, annealing at 55-64 ℃ for 1 min and elongation at 68 ℃ for 1 min per kb of plasmid length. A fraction (10 µl) of the PCR product was verified by 1% agarose gel electrophoresis, and the remaining reaction was digested with DpnI (10 U) at 37 ℃ for 2 h or overnight (O/N) to remove methylated parental DNA.

3.2 Agarose gel electrophoresis

Samples were mixed with 1x DNA loading dye and loaded onto a 1% agarose gel in 1xTAE stained with ethidium bromide (EtBr, 0.5 µg/ml). 2-log DNA ladder was used as a marker and the electrophoresis was run at 100 V for 45-60 min. The gel was imaged using BioRad GelDoc™ EZ Imager.

3.3 Transformation

3.3.1 XL1-Blue super-competent cells

25 µl *Escherichia coli (E. coli)* XL1-Blue super-competent cells were transformed with 2.2 µl of the digested PCR product (see section 3.1). The reaction was kept on ice for 25 min followed by heat shock at 42 ℃ for 45 sec. Cells were then left on ice for 2 min before recovering in 80 µl S.O.C medium for 1 h at 37 ℃ whilst shaking at 250 rpm. Cells were subsequently plated on an ampicillin (100 µg/ml) or kanamycin (50 µg/ml) containing LB-agar plate and incubated O/N at 37 ℃, followed by plasmid purification (see section 3.4).

3.3.2 BL-21 codon Plus (DE3)-RIL bacterial cells

30 ng of plasmid DNA encoding protein of interest was added to 6 µl of *E. coli* BL-21 Codon Plus (DE3)- RIL bacterial cells and incubated on ice for 15 min followed by heat shock for 45 sec at 42 ℃. Cells were left on ice for 2 min before recovering in 80 µl S.O.C medium for 1 h at 37 ℃ whilst shaking at 250 rpm. Cells were subsequently plated on an ampicillin (100 µg/ml) containing LB-agar plate and grown O/N at 37 ℃, before proceeding with protein expression and purification (see section 3.7).

3.4 Bacterial cultivation and mini prep plasmid purification

A colony was inoculated in 5 ml LB-medium containing ampicillin (100 µg/ml) or kanamycin (50 µg/ml) O/N at 37 ℃ whilst shaking at 250 rpm. The bacterial culture was spun down (5250 g for 10 min) and plasmid DNA was purified using NucleoSpin® Plasmid miniprep kit according to manufacturer's protocol for isolation of high-copy plasmid DNA from *E. coli,* including an additional washing step with buffer AW. For the elution of plasmid DNA, 25 µl of elution buffer AE (5mM Tris/HCl pH 8.5) was added and incubated for 3 min before centrifugation (11 000 g for 1 min). This step was then repeated for a total elution volume of 50 µl. The DNA concentration was measured by NanoDrop ND-1000™ Spectrophotometer and the sequence was verified by DNA sequencing. The purified plasmid DNA was stored at -20 ℃.

3.5 Measurement of DNA concentration and purity

The concentration and purity of the plasmid DNAs were measured using NanoDrop ND-1000™ spectrophotometer. The DNA concentration was determined by ultraviolet (UV) absorbance measurements, as DNA absorb light most strongly at a wavelength of 260 nm. The purity of the DNA sample was estimated by calculating the ratio of absorbance at A260 and A280 (260/280). Pure DNA should have a ratio about ∼1.8-1.9, and higher or lower ratios could be an indication of contaminations.

3.6 DNA sequencing

Purified plasmid DNA was sequenced following the BigDye v.3.1 protocol. The sequencing reaction included 400 ng of purified plasmid DNA, 1 µl of sequencing buffer, 0.5 µM of either forward or reverse primer, 1 µl of Big-Dye version 3.1 enzyme and ddH_20 to a final volume of

10 µl. The PCR cycles were run with an initial denaturation at 96 ℃ for 5 min followed by 27 cycles with denaturation at 96 ℃ for 10 sec, annealing at 50 ℃ for 5 sec and elongation at 60 ℃ for 4 min. Following the PCR, 10 µl of ddH_20 was added to the sequencing reaction and the sample was delivered to the university of Bergen (UiB) sequencing facility.

3.7 Expression and purification of GST-tagged recombinant proteins

A bacterial colony was inoculated in 5 ml LB-medium containing ampicillin (100 µg/mL) and incubated O/N at 37 ℃ whilst shaking at 250 rpm. 4 ml of the O/N culture was added to 200 ml LB-medium with ampicillin (100 µg/mL) and incubated at 37 ℃ while shaking (250 rpm) until the OD_{600} had reached about 0.6-0.8. The expression of the recombinant proteins was induced with isopropyl β-D-thiogalactopyranoside (IPTG, 0.5 mM) for 3 h at 37 ℃ or O/N at 15 ℃ (Fragment 2) whilst shaking at 250 rpm. Following the induction, the OD_{600} was measured. The bacterial culture was harvested by centrifugation at 6000 rpm for 20 min at 4 ℃, and the pellet was resuspended in 13 ml of 25 mM Tris pH 8.0-9.2, 500 mM NaCl, 0.5% Igepal and 1x bacterial protease cocktail inhibitor (added fresh) on ice. Cells were lysed by sonication on ice for 3x 1 min (10 sec on, 2 sec off with an amplitude of 30%) followed by centrifugation at 15 000 g for 40 min at 4 ℃. The lysate was added to 1.5 ml of 50% slurry glutathione-sepharose 4B and rotated O/N at 4 ℃. The following day, the glutathione resin was added to an Econo-Pac® Chromatography Column and allowed to settle for 45 min before the flowthrough was collected and the column was washed 3x with 15 ml of 50 mM Tris pH 8.0-9.2, 100 mM NaCl. The recombinant Glutathione-S-transferase (GST)-tagged protein was eluted 3x with 500 µl of elution buffer (50 mM Tris pH 8.0-9.2, 100 mM NaCl, 0.5 mM DTT, 10 mM reduced glutathione (added fresh)). The protein concentration was estimated at A280 using NanoDrop ND-1000™ spectrophotometer and the concentration was calculated using the theoretical extinction coefficients provided by ProtParam (Table 3.1). The purified proteins were stored at -80 ℃.

Table 3.1: ProtParam computed parameters for the purified proteins

Purified proteins	Molecular Weight (kDa)	Extinction coefficient ($M^{-1} \cdot cm^{-1}$)	Theoretical isoelectric point (PI)
GST-PARP1 F1	51.65	74425	8.15
GST-PARP1 F1 K84A K86L K87L	51.56	74425	7.25
GST-PARP1 F2	45.41	64330	7.66
GST-PARP1 F2 Δ221-236	43.48	64330	6.34
GST-PARP1 F2 Δ346-352	44.56	64330	6.33
GST-PARP1 F4 K505A K506A K508L	32.53	48610	6.36
GST-PARP1 F6	68.65	78075	6.73

3.8 SDS-PAGE

Sodium dodecyl sulphate-polyacrylamide gel electrophoresis (SDS-PAGE) was run to separate proteins according to their molecular weight and was performed to assess the purity of the purified proteins. Samples were prepared by adding 1x SDS sample buffer before heating the samples at 95 ℃ for 5 min. Samples were loaded onto a 12 or 13% polyacrylamide gel and the electrophoresis was carried out in 1x TGS buffer at 80 V until the samples had reached the resolving gel, before the voltage was increased to 120 V until the dye reached the bottom of the gel. The gel was further stained with InstantBlue™ (Coomassie protein stain) for 30-45 min with gentle agitation and imaged using the Bio-Rad GelDoc™ EZ Imager.

3.9 Lipid overlay assay

Binding of the recombinant GST-tagged PARP-1 WT and mutant proteins to different lipids was assessed using PIP Strips™ (Echelon Biosciences Inc.). These membranes are spotted with 15 lipids including the 7 PPIns. The membrane was blocked with 3% essentially fatty acid-free BSA in TBS-T (0.1% tween in TBS) for 1 h at room temperature (RT) with gentle agitation. 0.5 µg/ml of protein was added to the membrane and incubated for 1 h at RT with gentle agitation. The protein solution was then removed, and the membrane was washed 6x 5 min with TBS-T. The membrane was then incubated with anti-GST antibody conjugated to horse radish peroxidase (HRP) (1:30 000) in blocking buffer for 1 h at RT with gentle agitation before the membrane was washed as previously described. The bound protein was detected using

SuperSignal™ West Pico PLUS Chemiluminescent Substrate and imaged by ChemiDoc XRS+™.

3.10 Cell culture maintenance

3.10.1 Cell cultivation

HeLa- and MEF cells were cultivated in complete medium consisting of high glucose Dulbecco´s modified Eagle medium (DMEM), supplemented with 10% fetal bovine serum (FBS), and 1% penicillin/streptomycin (PS). Cells were maintained at 37 ℃ in a humidified 5% CO_2 incubator and passaged when reaching 70-90% confluence.

3.10.2 Cell passage

Cells were washed once with phosphate-buffered saline (1xPBS) and incubated with 1 ml of trypsin (0.25%) for 2 min at 37 ℃ and 5% CO_2 to detach the cells. Pre-warmed, complete medium was added, and cells were further resuspended and split into new 10 cm plates at various split ratios (1:4, 1:6 or 1:10) according to use.

3.10.3 Cell freezing

Cells were washed once with 1x PBS and trypsinized for 2 min at 37 ℃ and 5% CO_2 and then resuspended in 5 ml of pre-warmed complete medium. Cells were spun down (5 min, 900 rpm) and the medium was removed. The pellet was resuspended in 1 ml DMSO containing medium (90% complete medium, 10% DMSO) and added to a cryovial. Cells were frozen slowly at -80 ℃ using a Mr. Frosty™ Freezing Container, before they were moved to liquid nitrogen.

3.10.4 Cell thawing

Cells were thawed quickly at 37 ℃ and 6 ml of pre-warmed complete medium was added to dilute the DMSO which can be toxic for the cells. Cells were spun down at 900 rpm for 5 min and the medium was subsequently removed. The cell pellet was resuspended in 1 ml complete medium and transferred to a 10 cm dish.

3.11 Immunostaining

Actively growing cells were washed 2x with 1x PBS and fixed with 3.7% paraformaldehyde/PBS for 10 min at RT. Cells were then washed 3x with 1x PBS and permeabilized with 0.25% Triton-X100/PBS for 10 min at RT. After the permeabilization, cells were blocked with 5% goat serum in 0.1% Triton X-100/PBS for 1 h at RT before they were

incubated with primary antibody (Table 2.1.8) diluted in blocking buffer for 1 h at RT or O/N at 4 ℃. Following the incubation, cells were washed 4x 5 min with PBS-T (0.05%) using gentle agitation, and incubated with secondary antibody (Table 2.1.9) diluted in blocking buffer for 1 h at RT. Cells were subsequently washed 4x 5 min with PBS-T before the coverslip was dipped briefly in H_2O and mounted with ProLong® Glass antifade mountant with NucBlue on glass slides. Images were obtained by the Leica Fluorescence microscope DMI 6000 B using a 100 x/1.4 oil objective and Leica Application Suite Advanced Fluorescence software, including filters for detecting blue (A), red (TX2) and green (GFP) fluorescence.

3.12 H_2O_2 treatment

PAR-formation was induced by H_2O_2 treatment in order to determine PARP-1 activity. Cells were seeded 1:10 from a nearly confluent 10 cm dish on 12 mm coverslips in a 6-well plate and incubated O/N at 37℃ and 5% CO_2. The following day, the complete medium was replaced with FBS/PS free-medium and cells were treated with 1 mM H_2O_2 or medium-only (control) for 10 min at 37 ℃ and 5% CO_2. The medium was then aspirated, and cells were washed 2x with 1xPBS, and fixed with ice cold methanol: acetic acid (3:1) for 5 min on ice. For immunostaining, cells were blocked with 5% milk in PBS-T (0.05% Tween in PBS) for 1 h at RT as described in (Léger et al., 2014). The following steps of the immunostaining were performed as previously described (see section 3.11) and the mean PAR-intensity was quantified using ImageJ.

3.13 Multiple sequence alignment

A multiple sequence alignment (MSA) was created to examine the conservation among PIP_3 binding sites of PARP-1 orthologues. The MSA was generated using MUSCLE derived from EMBL-EBI (Madeira et al., 2019) and sequences for *Homo sapiens* (human; P09874), *Mus musculus* (mouse; P11103), *Bos taurus* (bovine; P18493), *Gallus gallus* (Chicken; P26446), *Xenopus laevis* (African clawed frog; P31669) and *Danio rerio* (zebrafish; Q5RHR0) were retrieved from UniProt knowledgebase (Consortium, 2018).

4 Results

4.1 PARP-1 binds to PI*P*$_3$ and other PPIns via three polybasic regions

To better understand the functional roles of PI*P*$_3$ in the nucleus, our group mapped the nuclear PI*P*$_3$ interactome using nuclear extracts from HeLa cells (Mazloumi Gavgani et al., 2017). Several potential PI*P*$_3$ binding proteins were identified and enriched in processes such as RNA processing, mRNA splicing and DNA repair. Many of the identified proteins were also annotated to the nucleolus, including PARP-1. PARP-1 was further shown to bind directly to PPIns, including PI*P*$_3$ and to colocalize with PI*P*$_3$ in the nucleolus of HeLa cells (Mazloumi Gavgani et al., 2017). One of the aims of this study was to determine the specific PI*P*$_3$ interaction sites on PARP-1.

PARP-1 does not contain any specific PPIn-binding domains; however, several PBRs or K/R motifs known to bind PPIns, have been found within the DBD and the AD of PARP-1 (Figure 4.1). The DBD consists of three zinc finger motifs (I-III), in which zinc finger I-II bind and recognize DNA structures, while zinc finger III mediates interdomain interactions. The AD consists of a BRCT domain which mediates protein-protein interactions. PARP-1 zinc finger I (aa 9-93) contains one K/R motif (^{78}**R**WDDQQ**K**V**KK**^{87}), while zinc finger III (aa 216-366) contains one large PBR in its N-terminal (^{221}**KKK**S**KK**E**K**D**K**DS**K**LE**K**^{236}) and a smaller PBR in its C-terminal (^{346}**KK**L**K**V**KK**^{352}). In addition, the linker region located in between the BRCT- and WGR domain contains a reverse K/R motif (^{505}**KK**S**K**GQV**K**^{512}).

To investigate whether the PBRs or K/R motifs found in PARP-1 are important for the interaction with PI*P*$_3$, four mutants were generated by site directed mutagenesis using GST-tagged recombinant PARP-1 fragments (Table 2.1.11). The two PBRs found in the N- and C-terminal of zinc finger III were deleted (Δ 221–236 and Δ346–351) in two separate mutants. In addition, three positively charged lysine residues in the K/R motifs found in the zinc finger I (^{84}**K**V**KK**^{87}) and in the linker region (^{505}**KK**S**K**^{508}) were mutated into the neutral, nonpolar amino acids alanine or leucine (Figure 4.1).

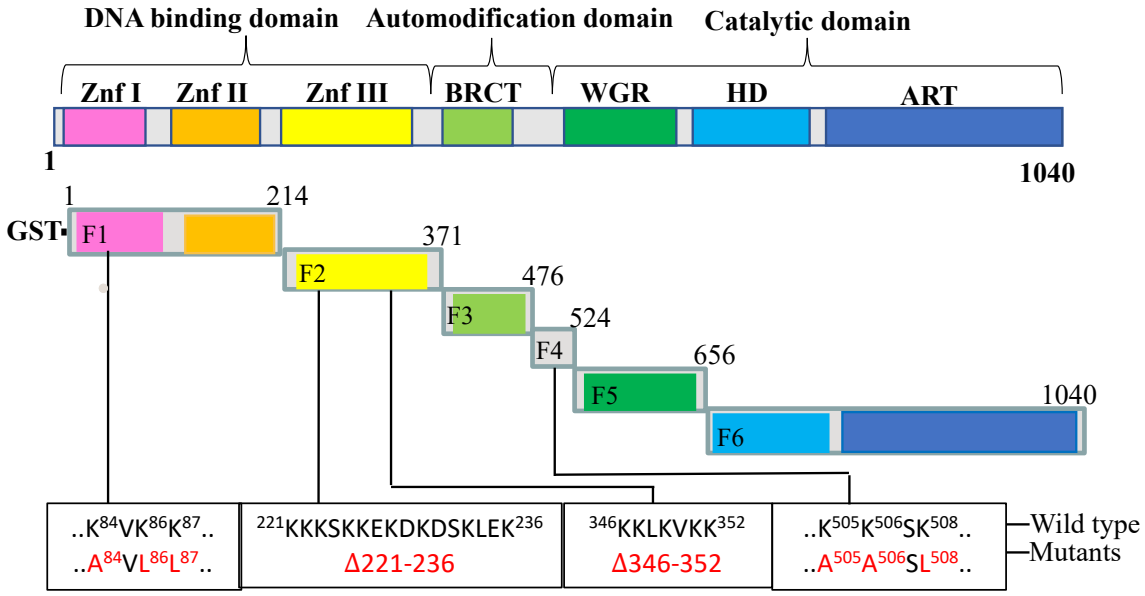

Figure 4.1: Overview of recombinant GST-PARP-1 mutants. Four mutants were generated by site directed mutagenesis using recombinant GST-PARP-1 fragments (F1-6). The two PBRs found in zinc finger III were deleted (F2), while three lysine residues in the K/R motifs found in zinc finger I (F1) and in the linker region (F4) were mutated into an alanine or leucine. Abbreviations: Znf I-III: zinc finger I-III, BRCT: BRCA1 C-terminal domain, WGR: Trp-Gly-Arg domain, HD: helical subdomain, ART: (ADP-ribosyl) transferase domain (ART) F1-F6: fragment 1-6.

Protein expression and purification

GST-PARP-1 fragment mutants, in addition to PARP-1 fragment 1-2 and fragment 6 WTs were expressed in *E. coli* BL-21 Codon Plus (DE3)- RIL cells and purified using glutathione sepharose 4B beads. The expression and purification of the proteins were analysed by SDS-PAGE followed by Coomassie blue staining (Figure 4.2). The protein bands corresponded to the expected molecular weight for all proteins (Table 3.1). PARP-1 fragment 1 WT (aa 1-214) and mutant had low protein expression but high purity (Figure 4.2 A and B), while PARP-1 fragment 2 WT (aa 215-371) and mutant proteins (Figure 4.2 C-E) showed high protein expression levels but also some impurities and/or degradation. High protein expression levels were also observed for fragment 4 mutant (aa 477-524) and fragment 6 WT (aa 656-1014) (Figure F-G). A band corresponding to the GST-tag (26 kDa) was observed for all proteins except for fragment 1 WT and mutant proteins.

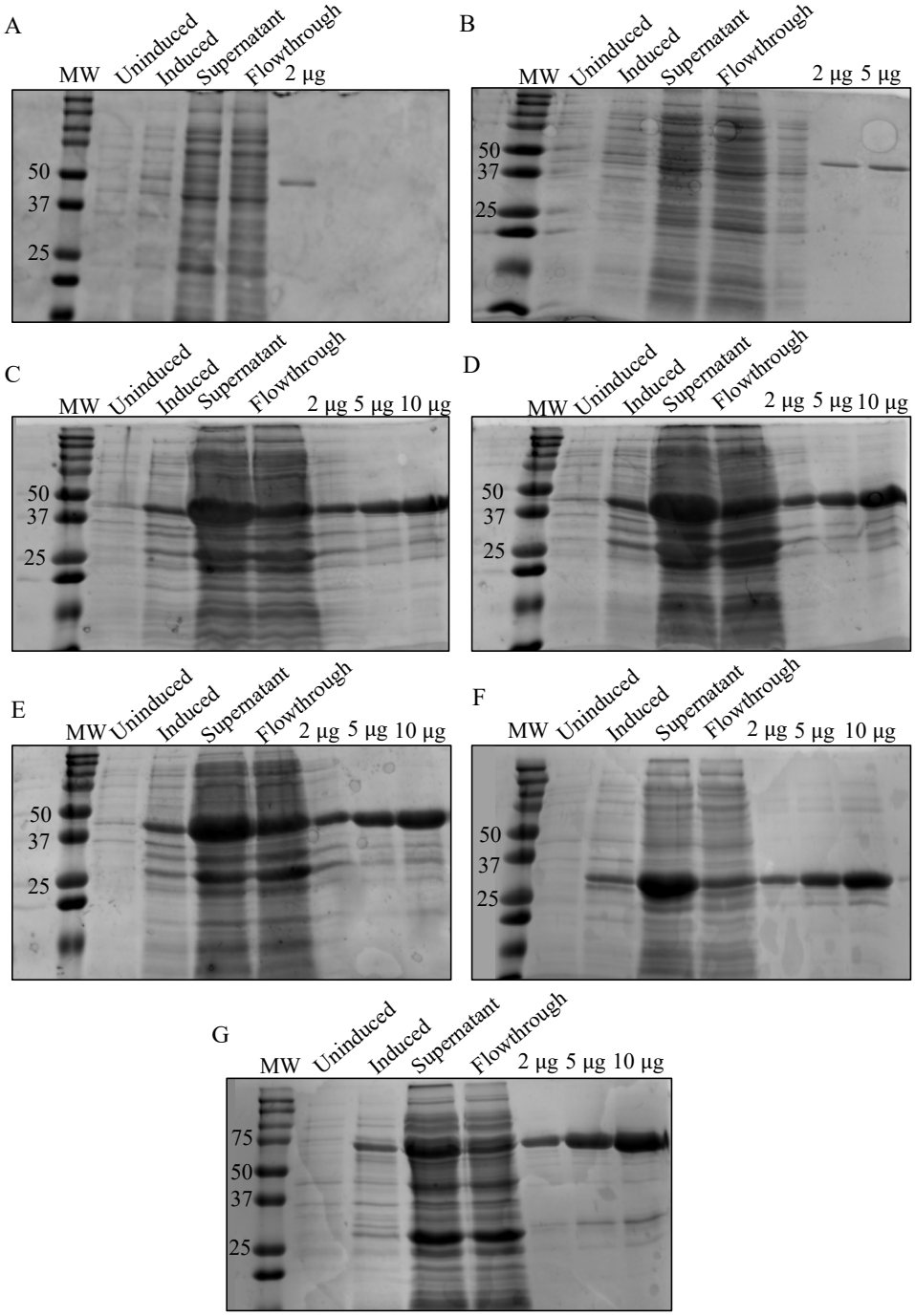

Figure 4.2: Expression and purification of GST-tagged recombinant PARP1 WT and mutant proteins. Expression and purification of **A)** GST-PARP-1 fragment 1 WT (1-214), **B)** GST-PARP-1 fragment 1 K84A-K86L-K87L mutant, **C)** GST-PARP-1 fragment 2 WT (215-371), **D)** GST-PARP-1 fragment 2 Δ221-236 mutant, **E)** GST-PARP-1 fragment 2 Δ346-352 mutant, **F)** GST-PARP-1 fragment 4 (477-524) K505A-K506A-K508L mutant, and **G)** GST-PARP-1 fragment 6 WT (657-1014). Proteins were expressed using BL-21 Codon Plus (DE3)- RIL bacterial cells which were induced with 0.5 mM IPTG for 3 h at 37℃ (or overnight at 15℃ for fragment 2). Proteins were subsequently purified using glutathione-sepharose beads. The protein concentration was estimated at A280 using NanoDrop ND-1000™ Spectrophotometer and the concentration was calculated using the theoretical extinction coefficients provided by ProtParam. Samples from uninduced, induced, supernatant, flowthrough and purified proteins were loaded onto an SDS-PAGE for analysis and stained with InstantBlue™ Coomassie staining. Precision Plus Protein™ standard was used as a marker and the gel was imaged using the Bio-Rad GelDoc™ EZ Imager.

Binding of PARP-1 fragments WT and mutant proteins to PPIns

A lipid overlay assay was used to investigate the lipid binding affinity of GST-PARP-1 fragments WT and mutant proteins. A variety of lipids including all seven PPIns were spotted on a hydrophobic membrane and incubated with the recombinant GST-PARP-1 proteins. The bound proteins were subsequently detected using anti-GST antibody conjugated to HRP. PARP-1 fragment 1 (Zinc finger I & II, aa 1-214) bound with high affinity to PtdIns3*P* and with lower affinity to the other PPIns. However, no binding was observed for PtdIns(3,4)P_2 or PIP_3 (Figure 4.3B). The fragment 1 triple mutant (^{84}AVLL^{87}) did not show any significant decrease in its binding affinity compared to the WT, indicating that the K/R motif within Zinc finger I and II is not important for the binding of PtdIns3*P* nor the other PPIns which binds weakly (Figure 4.3B). However, both PARP-1 fragment 2 (zinc finger III) and fragment 4 (linker region) bound to PIP_3. PARP-1 fragment 2 WT (aa 215-371) also bound to other PPIns with various binding affinities and to lysophosphatic acid (LPA), phosphatic acid (PA) and phosphatidylserine (PS). PARP-1 fragment 4 WT (aa 477-524) bound to all PPIns except for PtdIns(3,4)P_2 and to PA. PARP-1 fragment 2 and fragment 4 mutants showed a reduced binding affinity to PPIns, indicating that these binding sites are important for PPIn binding. Two distinct mutants were generated for PARP-1 fragment 2 (zinc finger III), where either amino acids 221-236 or 346-352 were deleted. The Δ221-236 mutant had a very weak binding affinity for the mono-phosphorylated PPIns. The Δ346-352 mutant showed some binding to the mono-phosphorylated PPIns and to PA, while a very weak binding affinity was observed for PtdIns(3,4)P_2 and PtdIns(4,5)P_2. Both mutants did however completely lose their binding affinity to the other lipids including PIP_3 (Figure 4.3 C). Two mutants were generated for PARP-1 fragment 4 (linker region). The double mutant (^{505}AASK^{508}) showed clearly reduced binding affinity for the mono-phosphorylated PPIns and to PA, while it did no longer bind to PtdIns(3,5)P_2, PtdIns(4,5)P_2 or to PIP_3. The triple mutant which had an extra lysine residue mutated into a leucine (^{505}AASL^{508}) showed no binding to either of the PPIns and only had a very weak binding affinity to PA (Figure 4.3 D).

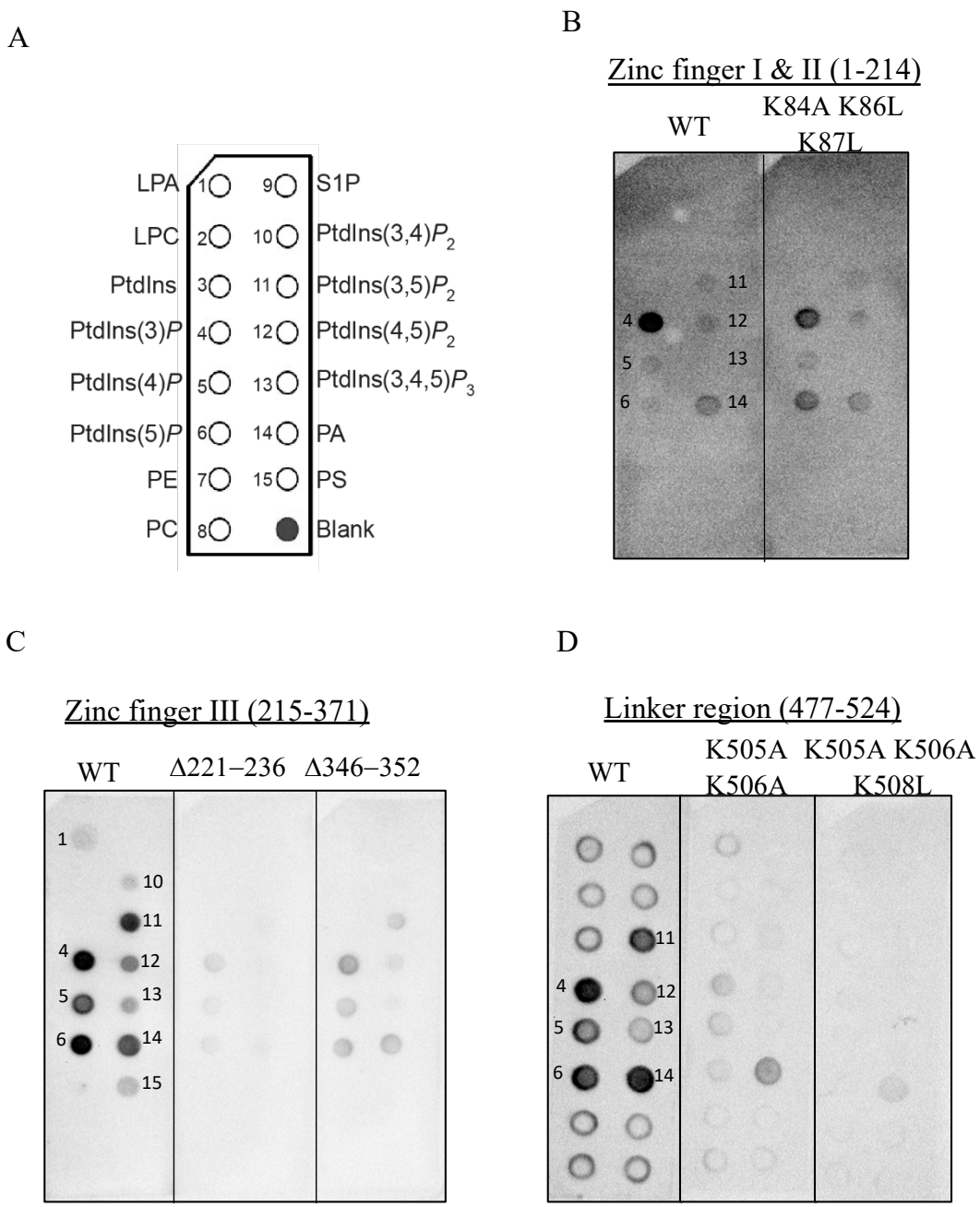

Figure 4.3: Interaction of GST-PARP-1 fragments WT and mutant proteins with PPIns. A) Schematic representation of lipids spotted (100 pmol) on a hydrophobic membrane (PIP strips, Echelon Biosciences) including Lysophosphatic acid (LPA), Lysophosphocholine (LPC), Phosphatidylinositol (PtdIns), PtdIns3*P*, PtdIns4*P*, PtdIns5*P*, Phosphatidylethanolamine (PE), Phosphatidylcholine (PC), Sphingosine-1-Phosphate (S1P), PtdIns(3,4)P_2, PtdIns(3,5)P_2, PtdIns(4,5)P_2, PtdIns(3,4,5)P_3, Phosphatic acid (PA), Phosphatidylserine (PS) and Blank. Lipid overlay assay of **B)** GST-PARP-1 fragment 1 WT (1-214) and mutant, **C)** GST-PARP-1 fragment 2 (215-371) WT and deletion mutants, and **D)** GST-PARP-1 fragment 4 WT (477-524) and mutants. All PIP-strips were incubated with 0.5 µg/ml of GST- PARP-1 proteins for 1 hour at RT and the bound proteins were detected using anti-GST antibody conjugated to HRP and SuperSignal™ West Pico PLUS Chemiluminescent Substrate. Lipid blots were imaged by ChemiDoc XRS+™ with 10 sec exposure time.

4.2 Sequence conservation among the PIP_3 binding sites

To determine whether the PBR or K/R-motifs that were shown to bind PPIns, including PIP_3 are conserved among vertebrate species, we carried out a multiple sequence alignment. An alignment of the PBR/ KR motifs of PARP-1 in vertebrate species including *Homo sapiens* (human; P09874), *Mus musculus* (mouse; P11103), *Bos taurus* (bovine; P18493), *Gallus gallus* (Chicken; P26446), *Xenopus laevis* (African clawed frog; P31669) and *Danio rerio* (zebrafish; Q5RHR0) was performed using the alignment tool MUSCLE (Madeira et al., 2019). The PBRs found in the zinc finger III showed conservation among the vertebrate species (Figure 4.4A). However, some modification of the N-terminal PBR was observed in the sequence of *Danio rerio*. Meanwhile, the K/R motif found in the linker region only showed conservation among the mammals, while the sequences of *Gallus gallus*, *Xenopus laevis* and *Danio rerio* did not follow the consensus of the K/R motif sequence (K/R-K/R-X-K-($X_{n=3-7}$)-K/R) (Figure 4.4A). Examination of the zinc finger III structure (aa 225-359, PDB: 2RIQ) revealed that the N-terminal PBR (aa 221-236) is part of an α-helix that extends away from the rest of the motif, while the C-terminal PBR (aa 346-352) is located at the end of an α-helix and extends into an unstructured tail (Figure 4.4B).

A

H. Sapiens	^{221}KKKSKKEKDKDSKLEK^{236}	^{346}KKLKVKK^{352}	^{505}KKSKGQVK^{512}
M. Musculus	^{221}KKKSRKETDKYSKLEK^{236}	^{346}KKLKVKK^{352}	^{504}KKSKGCFK^{511}
B. Taurus	^{224}KKKSKKEKDKEIKLEK^{239}	^{349}KKLKIKK^{355}	^{507}KKSKGPVK^{514}
G. Gallus	^{220}KKKSRKEKEKESKQEK^{235}	^{345}KKFKCKK^{351}	^{501}MKSAGKVK^{508}
X. Laevis	^{207}KKKIKKEKEKESKLEK^{222}	^{331}KKFKFKR^{338}	^{487}GKSSGKVK^{494}
D. Rerio	^{219}-GVSKKQKKEDEKLEQ^{230}	^{340}KKFKFKR^{346}	^{504}SKSTGKVK^{511}

B

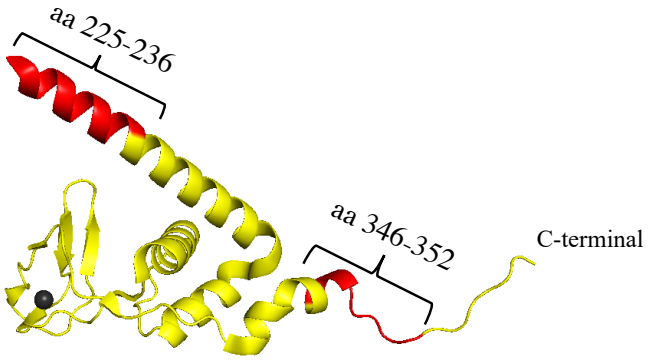

Figure 4.4: A) Multiple sequence alignment (MSA) of the two polybasic regions (PBRs) found in the zinc finger III and the K/R motif found in the linker region of human PARP-1 compared to other vertebrate species. The MSA was performed by the alignment tool MUSCLE (Madeira et al., 2019). Accession number for; *Homo sapiens* (P09874), *Mus musculus* (P11103), *Bos taurus* (P18493), *Gallus gallus* (P26446) *Xenopus laevis* (P31669), *Danio rerio* (Q5RHR0). The positively charged amino acid residues are highlighted in red. **B)** Crystal structure of human PARP-1 zinc finger III (aa 225-359, PDB: 2RIQ**).** The PBRs found in the N-terminal (aa 221–236) and C-terminal (aa 346–352) of PARP-1 zinc finger III are highlighted in red.

4.3 PARP-1 harbours a potential NoLS

Previous studies have shown that PARP-1 localizes to the nucleolus (Meder et al., 2005), and this was also confirmed in the present study. Immunofluorescence staining with anti-PARP-1 and anti-NPM antibodies, showed that PARP-1 colocalizes with NPM, a nucleolar marker, in HeLa cells (Figure 4.5A). No nucleolar localization signal (NoLS) responsible for targeting PARP-1 to the nucleolus has so far been identified. The nucleolar localization signal has no consensus sequence, but it is often found to include short stretches rich in arginine and/or lysine residues (Scott et al., 2010), which is similar to that of the NLS and for PPIns binding. It would therefore be interesting to investigate whether any of the PBRs in PARP-1 that binds PPIns could potentially harbour an NoLS.

Nucleolar localization sequence detector (NoD) is an online tool that predicts NoLS in proteins (Scott et al., 2011). The human PARP-1 primary sequence (P09874) was analysed by the NoD, which detected one potential NoLS (Figure 4.5B). The predicted NoLS consisted of the following sequence ^{216}VDEVA**KKKSKKEKDKDSKLEK**ALKA^{240} located in the PARP-1 zinc finger III motif (aa 216-366). Interestingly, both the N-terminal PBR that binds PIP_3 (aa 221-236) and the NLS (aa 207-226) were shown to be part of the predicted NoLS.

A

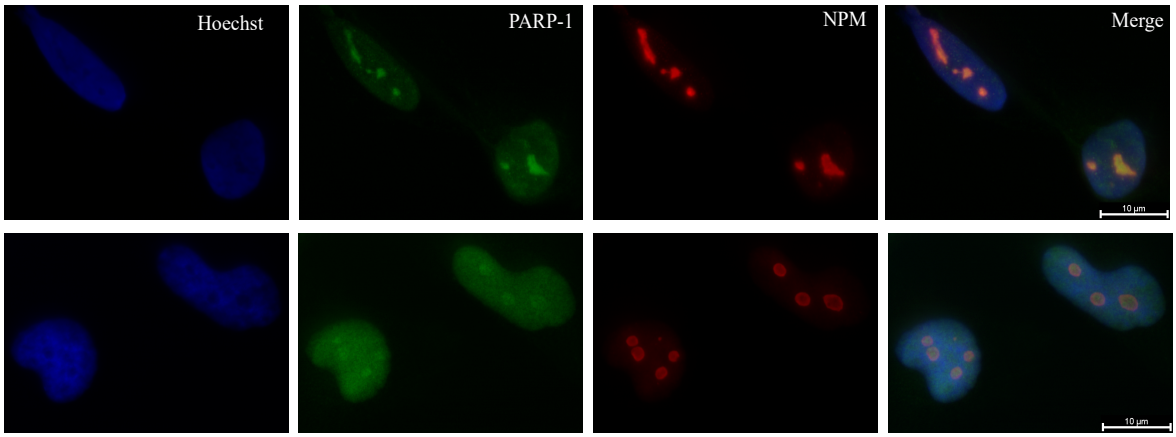

B

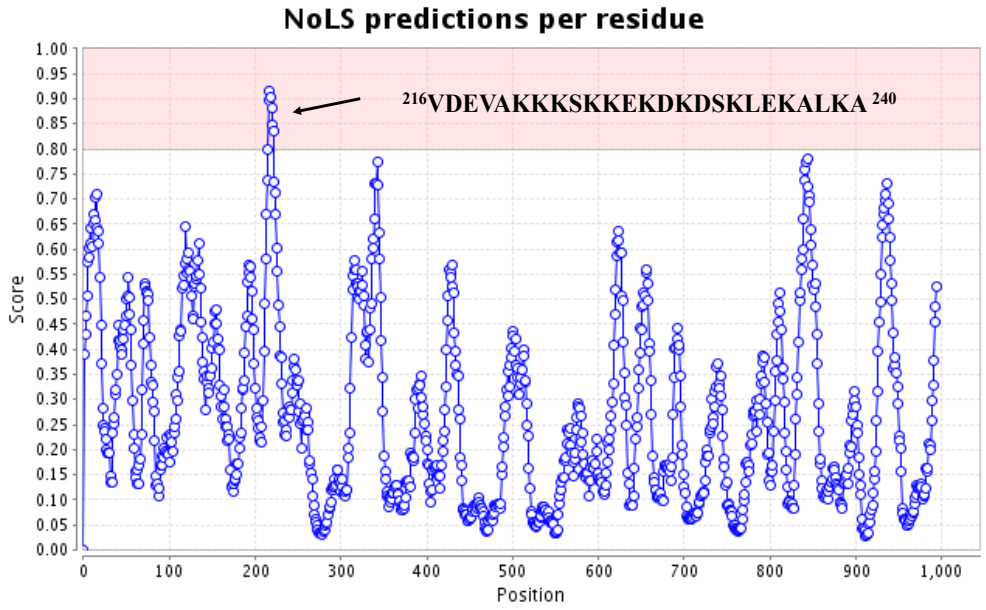

Figure 4.5: PARP-1 localizes to the nucleolus. A) HeLa cells were stained with anti-PARP-1 and anti-NPM antibodies, and the cell nuclei were stained with ProLong® Glass antifade mountant with NucBlue. Cells were imaged by Leica Fluorescence microscope DMI 6000 B. Scale bar represents 10 µm. **B)** One NoLS (aa 216-240) was predicted in human PARP-1 (P09874) using the Nucleolar localization sequence Detector (NoD) algorithm (Scott et al., 2011). Abbreviations: PARP-1: poly(ADP-ribose) polymerase-1, NPM: nucleophosmin, NoLS: nucleolar localization signal.

4.4 H_2O_2 induced PAR formation is not dependent on p110β activity

PARP-1 enzymatic activity is induced in response to DNA damage, which results in the PARylation and recruitment of proteins required for DNA repair (Wei and Yu, 2016). To investigate whether PIP_3 regulates PARP-1 function in response to DNA damage, the effect of H_2O_2 induced DNA damage on PARylation was examined in MEF cells harbouring WT or kinase dead version of class I PI3K p110β (one of the enzymes responsible for PIP_3 synthesis and is also known to be present in the nucleolus (Gavgani et al., 2019)).

To do so, cells were treated with H_2O_2, a genotoxic agent that is known to induce DNA damage, or left untreated followed by fixation and immunostaining with antibodies against PAR. In the first experiment, high levels of PAR background staining were observed in the cytoplasm in both untreated and treated cells (Figure 4.6A). PARP-1´s basal enzymatic activity is known to be very low, but increase dramatically upon activation such as DNA strand breaks (Kim et al., 2005) and it was therefore hypothesized that the fixation method for immunofluorescence staining which included 10 min of incubation with 3.7% paraformaldehyde (PFA) at RT could mediate artificial PAR staining.

Using HeLa cells, two other fixation methods were tested upon the same H_2O_2 treatment. Cells were either fixed with 100% methanol for 10 min at -20 ℃ or they were fixed with methanol: acetic acid (3:1) for 5 min on ice. The two first mentioned fixation methods (3.7% PFA and 100% methanol) were also followed by blocking with 5% goat serum in 0.1% triton x100/PBS, while the latter one was blocked with 5% milk in PBS-T (0.05% tween) as described in (Léger et al., 2014). Cells fixed with either 100% methanol or with methanol: acetic acid (3:1) showed a high reduction in background staining compared to cells fixed with 3.7% PFA (Figure 4.6B). The PAR staining of the treated cells also showed to be mostly located in the nucleus, where PARP-1 localizes (Figure 4.6B). As the best results were obtained from cells fixed with methanol: acetic acid (3:1), this fixation method was used for further experiments.

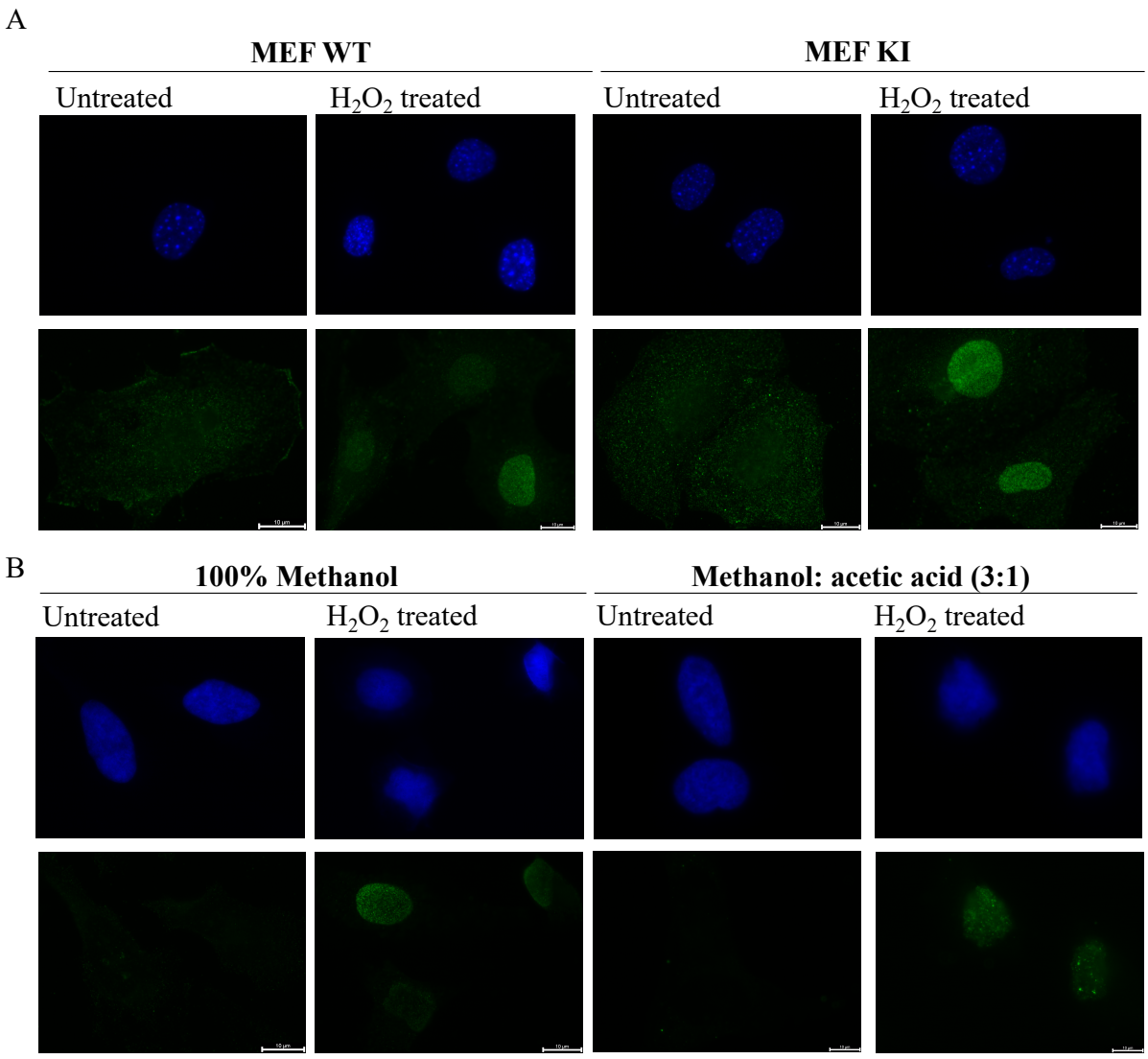

Figure 4.6: A) Effect of different fixation methods in PAR staining in H_2O_2 treated cells. **A)** MEF cells harbouring WT or kinase dead version of class I PI3K isoform p110β (KI) were untreated or treated with 1 mM H_2O_2 for 10 min at 37 ℃ and 5% CO_2. Cells were then fixed with 3.7% paraformaldehyde for 10 min at RT. **B)** HeLa cells were either untreated or treated with 1 mM H_2O_2 for 10 min at 37℃ and 5 % CO_2 and then fixed with either 100% methanol for 10 min at -20 ℃ or with methanol: acetic acid (3:1) for 5 min on ice. Cells were stained with anti-PAR H10 antibody and cell nuclei were stained with ProLong® Glass antifade mountant with NucBlue. Cells were imaged by Leica Fluorescence microscope DMI 6000 B. Scale bar represents 10 μm.

MEF cells harbouring WT or kinase dead version of the PI3K isoform p110β were subsequently treated with the same H_2O_2 treatment followed by fixation with methanol: acetic acid (3:1) for 5 min on ice and blocked with 5% milk in PBS-T (0.05% tween) followed by immunostaining with anti-PAR H10 and anti-fibrillarin (nucleolar marker) antibodies (Figure 4.7A). A simple quantification of the mean PAR-signalling intensity in the nucleus was performed using ImageJ (Figure 4.7B). These data showed that the overall PAR-intensity in the nuclei was similar for both cell lines. When analysing the images, PAR and fibrillarin were shown to colocalize at small intense foci, but no large variations were observed in the two cell lines.

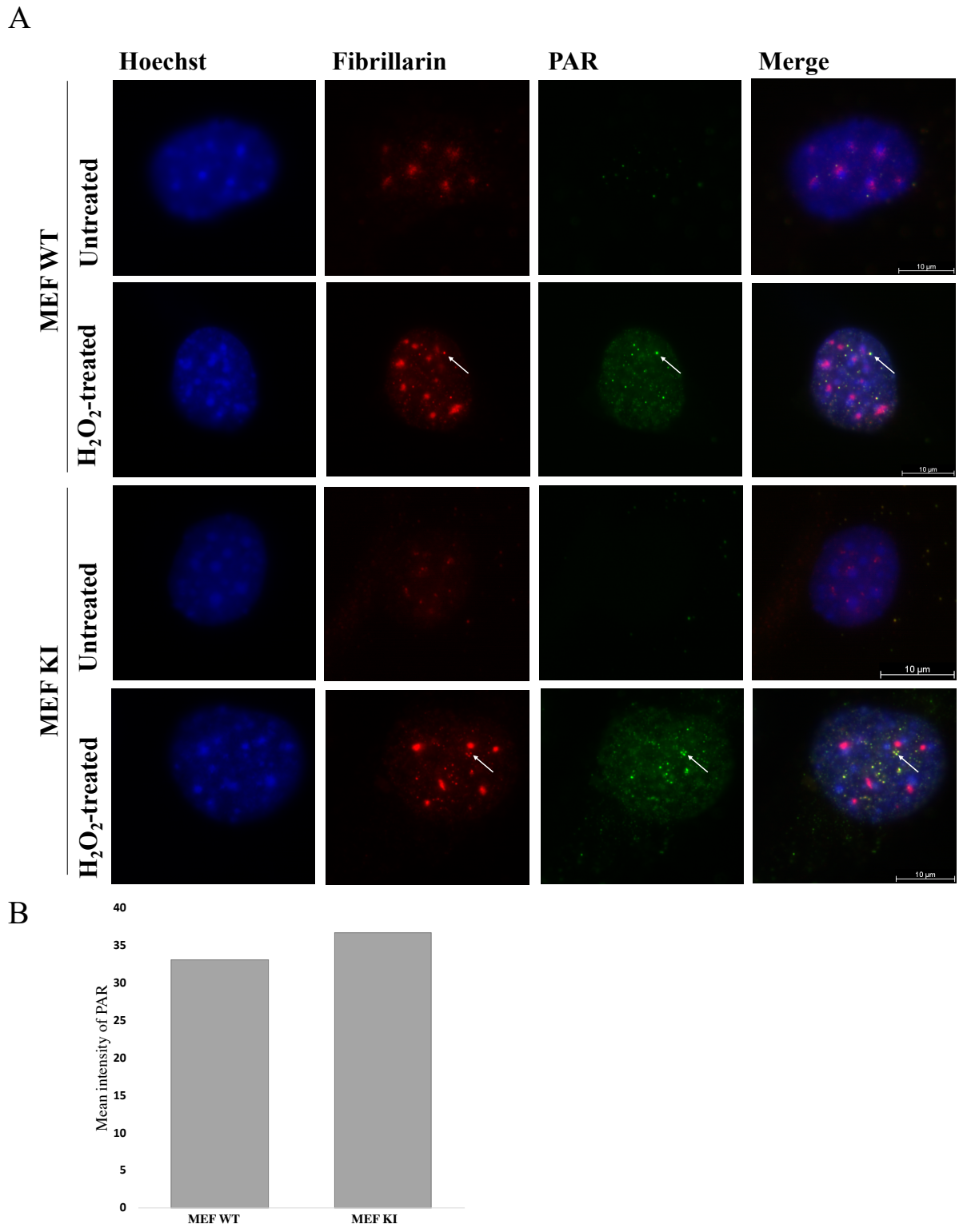

Figure 4.7: H_2O_2 treated MEF cells harbouring WT or kinase dead version of class I PI3K p110β (KI). A) Cells were untreated or treated with 1mM H_2O_2 for 10 min at 37 ℃ and 5% CO_2 and then fixed with methanol: acetic acid (3:1) for 5 min on ice and subsequently immunostained with anti-PAR and anti-fibrillarin antibodies. The cell nuclei were stained with ProLong® Glass antifade mountant with NucBlue and cells were imaged by Leica Fluorescence microscope DMI 6000 B. Scale bar represents 10 µm. **B)** Mean intensity of PAR-signal in nuclei was quantified using ImageJ. The data presented are only based on one replicate.

5 Discussion

The PI3K pathway is important for many cellular processes and several members of this pathway have been observed within the nucleus over the past years (Jacobsen et al., 2019). Our group has shown that the class I PI3K subunit p110β and its lipid product, PIP_3, localizes to the nucleoplasm and the nucleolus (Karlsson et al., 2016, Gavgani et al., 2019). However, only a few nuclear PIP_3 binding proteins have been identified and characterized so far. To better understand the functional role of PIP_3 in the nucleus, the nuclear PIP_3 interactome was mapped using isolated nuclei of HeLa cells in a quantitative mass spectrometry-based approach (Mazloumi Gavgani et al., 2017). Several potential PIP_3 binding proteins enriched in processes such as RNA processing, mRNA splicing, and DNA repair were identified (Mazloumi Gavgani et al., 2017). Additionally, many of the identified proteins were annotated to the nucleolus. PARP-1 was identified as a potential PIP_3 binding protein and our group decided to look further into their interaction, due to the reported nucleolar localization of PARP-1. The preliminary studies showed that PARP-1 interacts directly with PIP_3 and other PPIns using lipid overlay assay, as well as PARP-1 co-localized with PIP_3 in the nucleolus in HeLa cells (Mazloumi Gavgani et al., 2017).

In the present study, we investigated the specific PIP_3 interaction sites of PARP-1 by generating GST-tagged mutant fragments of PARP-1. We showed that two conserved PBRs found in the zinc finger III motif and one reverse K/R motif found in the linker region between the BRCT- and the WGR domain were important for interactions with PPIns, including PIP_3. Furthermore, the online tool NoD predicted one NoLS (aa 216-240) in the N-terminal of zinc finger III. This study also aimed to investigate whether PIP_3 regulated the enzymatic activity of PARP-1 upon H_2O_2 induced DNA damage, using MEF cells harbouring WT or kinase dead version of class I PI3K p110β. However, no major differences in PAR intensities were observed among the different cell lines upon this treatment.

5.1 PARP-1 binds PIP_3 via two PBRs and one K/R motif

Recombinant GST-tagged PARP-1 (full length) has previously been shown to interact directly with all PPIns except for PtdIns(3,4)P_2 as well as with PA and PS using lipid overlay assay (Mazloumi Gavgani et al., 2017). Here, we aimed to further determine the exact PIP_3 interaction sites of PARP-1 using recombinant GST-PARP-1 fragments. Two PBRs found in the zinc finger III and one reverse K/R motif found in the linker region between the BRCT- and the WGR domain were shown to be important for PPIn interaction, as deletion of either of the PBRs or mutation of three lysine residues into an alanine or leucine in the linker region, reduced or completely abolished the binding of PARP-1 to PPIns including PIP_3 (Figure 4.3). Nuclear interactomes studies of PtdIns(4,5)P_2 and PIP_3, respectively, have shown that many of the potential PPIn-binding proteins harbour at least one K/R motif, indicating that this is a common interaction site for nuclear PPIns (Lewis et al., 2011, Mazloumi Gavgani et al., 2017). These results are also consistent with the observation of other nuclear PPIn-binding proteins. SAP30/SAP30L, pf1, ING2 (Inhibitor of growth protein 2), TAF3 (TATA box binding protein-associated factor 3) and UHRF1 (Ubiquitin-like with PHD and RING finger domains 1) have all shown to bind various mono-phosphorylated PPIns via PBRs (Viiri et al., 2009, Gozani et al., 2003, Stijf-Bultsma et al., 2015, Gelato et al., 2014). Interestingly, some of these PBRs lies C-terminally of either a zinc-coordinating motif (SAP30L) or a PHD zinc finger (pf1, ING2, TAF3), similar to PARP-1 PBRs, which are found in the N-terminal and C-terminal region of zinc finger III. Moreover, PHF8 (PHD finger protein 8) and EBP1 bind to PtdIns(4,5)P_2 and PIP_3, respectively, via either a K/R motif or a PBR in the nucleolus (Ulicna et al., 2018, Karlsson et al., 2016), providing evidence for a nucleolar role of PPIns.

PARP-1 has been shown to interact with PPIns via lysine/arginine rich stretches through electrostatic interactions, and therefore, it is a possibility that the positively charged amino acids in the PARP-1 fragments could become more available for interactions compared to full length PARP-1, as the overall folding of the protein might be different. Thus, the PARP-1 fragments used in this study could contribute to non-specific binding between the fragments and lipids using lipid overlay assays. In the present study, PARP-1 fragment 2 WT (aa 215-371) bound to all PPIns as well as PA, PS and LPA. When a similar lipid overlay assay was performed for full length hPARP-1 (1-1040), it did not bind to PtdIns(3,4)P_2 nor LPA (Mazloumi Gavgani et al., 2017). This demonstrates that the fold and structure of the fragments differ from the same areas as in full length PARP-1. Additionally, the PPIns spotted on the hydrophobic membranes of the

lipid blots do not resemble the physiological condition of nuclear PPIns and PARP-1 might bind differently to PPIns in cells.

5.2 The PBRs in zinc finger III are conserved among vertebrates

In the present study, we showed that the two PBRs found in zinc finger III are conserved among vertebrate species (Figure 4A). Some variations were observed among the hydrophobic amino acids; however, the basic amino acid residues were highly conserved, providing evidence that these amino acid residues are functionally important for PARP-1. The reverse K/R motif found in the linker region only showed conservation among mammals. However, all vertebrate species examined, still harboured at least three lysine residues within the region, which could still be important for PPIn-binding, although they do not follow the consensus sequence of the K/R motif (K/R-(X_{3-7})-K-X-K/R-K/R). Furthermore, we examined the structural features of the PBRs found in the zinc finger III (Figure 4.4B). The PBRs are found at the N-terminal α-helix and C-terminal unstructured region of the zinc finger III which both extends away from the rest of the motif, indicating that these PBRs might be accessible for interactions with molecules such as PPIns.

5.3 A potential nucleolar localization signal identified in PARP-1

Several studies have shown that PARP-1 accumulates in the nucleolus, however, no nucleolar localization signal has been identified so far (Fakan et al., 1988, Meder et al., 2005). The NoLS does not follow a specific consensus sequence, but it is often found to include small stretches rich in positively charged amino acids such as lysine and arginine residues (Scott et al., 2010). We have shown that PARP-1 binds to PPIns via two PBRs and it would therefore be interesting to investigate whether any of these PBRs could potentially act as an NoLS and thus be responsible for targeting PARP-1 to the nucleolus. We used the online tool, NoD, to identify potential NoLS sequences in PARP-1. Using the full-length sequence of human PARP-1 (P09874), the NoD predicted one NoLS (aa 216-240) in the zinc finger III, which includes the N-terminal PBR (aa 221-236) which binds PPIns (Figure.4.5B). In addition, the first part of this sequence is also part of the NLS (aa 207-226), that is responsible for the nuclear localization of PARP-1 (Schreiber et al., 1992). These findings indicate that the PBR (221-236) is important for both the localization of PARP-1 to the nucleus and possible the nucleolus, and for its binding with PPIns, including PIP_3. This type of multifunctional role has also been observed among

other PPIn binding proteins. For example, the PPIn-binding site found in SAP30L is also part of an NLS, while the C-terminal PBR found in EBP1 is important for both PPIn-binding and for its localization to the nucleolus (Viiri et al., 2009, Karlsson et al., 2016).

PARP-2 is a closely related protein of PARP-1 and a previous study has shown that PARP-2 accumulates to the nucleolus by the presence of an NoLS (^{4}RRRR^{7}) (Meder et al., 2005). PARP-1 and PARP-2 activities are both induced upon DNA strand breaks and the enzymes are both involved in DNA repair pathways such as SSBR, where they have several common binding partners such as XRCC1, DNA ligase III and DNA polymerase β (Schreiber et al., 2002). The two enzymes have also been shown to bind the nucleolar protein NPM and they both localizes to the nucleolus independently of each other (Meder et al., 2005). Based on these similarities, one could reason that PARP-1 is targeted to the nucleolus by an NoLS in a similar manner to PARP-2. However, despite their similar functions, they display distinct N-terminal regions and only the catalytic domains are evolutionary conserved (Figure 5.1), suggesting that a potential NoLS in PARP-1 might have evolved independently of PARP-2.

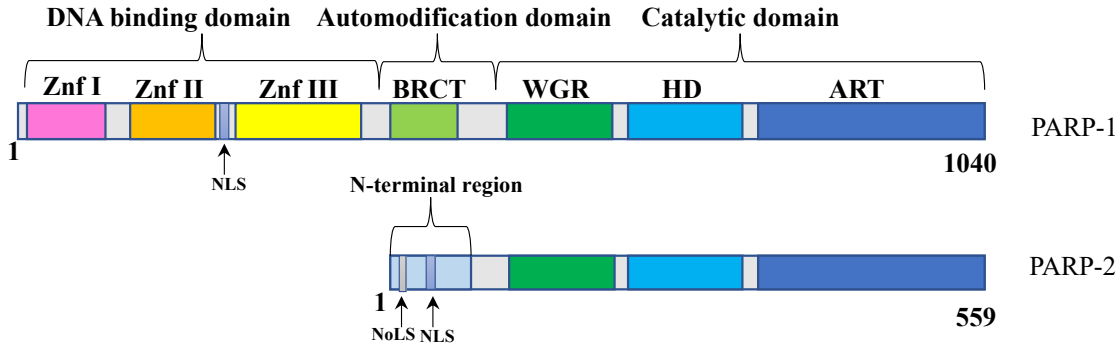

Figure 5.1 Schematic representation of PARP-1 and PARP-2 structures. PARP-1 and PARP-2 share a conserved catalytic domain, while their N-terminal regions are dissimilar. Beside the catalytic domain, PARP-1 consists of three zinc fingers (I-III), an NLS (aa 207-226) and a BRCT-domain. PARP-2 consists of a small N-terminal region which harbours an NoLS (aa 4-7) and an NLS (aa 35-40). Abbreviations: ZnI-ZnIII: zinc finger I-III, BRCT: BRCA1 C-terminal domain, WGR: Trp-Gly-Arg domain, HD: helical subdomain, ART: (ADP-ribosyl) transferase domain, NLS: nuclear localization signal, NoLS: nucleolar localization signal, PARP: poly(ADP-ribosyl) polymerase.

Even though an NoLS in PARP-1 has been predicted using the NoD, it has to be taken into account that it is only a prediction tool based on previously determined NoLS (Scott et al., 2011). Moreover, the NoD predicts the NoLS based on the primary sequence and it does not take into account for the three-dimensional structure of the protein. Thus, the NoLS predicted in PARP-1 needs to be validated experimentally.

Alternatively, PARP-1 could also interact with a nucleolar protein that harbours an NoLS, and in that manner be shuttled into the nucleolus by a nucleolar binding partner. Indeed, PARP-1 has been shown to interact with the nucleolar protein NPM, and previous studies have shown that interaction with NPM is necessary for the nucleolar localization of certain proteins (Korgaonkar et al., 2005, Li et al., 1996). It could therefore be interesting to investigate whether PARP-1´s nucleolar localization is altered or not in the absence of NPM.

5.4 H_2O_2 induced PAR formation is not dependent on p110β activity

PARP-1 enzymatic activity is induced in response to DNA damage which results in the PARylation and recruitment of proteins required for DNA repair (Ray Chaudhuri and Nussenzweig, 2017). In addition, both class I PI3K p110β and PIP_3 have been shown to mediate DNA repair in response to DSB (Kumar et al., 2010, Wang et al., 2017). Therefore, we wanted to investigate whether PIP_3 is important for regulating the enzymatic activity of PARP-1 in response to H_2O_2 induced DNA damage. For this purpose, we compared the mean PAR intensity in MEF cells harbouring WT or kinase dead version of class I PI3K kinase p110β. No large differences in PAR-intensities were observed between the two cell lines, indicating that the p110β activity or its lipid product, PIP_3 do not alter PARP-1´s function upon the H_2O_2 treatment used in this study (Figure 4.7).

PARP-1 is known to be activated upon both SSB and DSB, while studies have shown that p110β and PIP_3 mediate DSBR (Ray Chaudhuri and Nussenzweig, 2017, Kumar et al., 2010). SSBs are the most common type of DNA damage and studies have shown that H_2O_2 induced DNA damage mostly creates SSBs (Ismail et al., 2005). The levels of nuclear PIP_3 has been shown to increase upon H_2O_2 treatment, but with an H_2O_2 concentration of 10 mM, which is much higher than the concentration used in this study (1 mM) (Tanaka et al., 1999). It could therefore be a possibility that the DNA repair pathways that involves p110β or PIP_3 might not have been activated upon the H_2O_2 treatment used in the present study. Moreover, p110β has been shown to mediate DSB repair both through its activity and through a kinase-independent p110β function (Kumar et al., 2010). Kumar *et al*. showed that inhibition of the p110β kinase activity only delayed the DNA damage response, while deletion of the kinase almost abolished it, indicating that p110β is most critical in this pathway through a kinase independent function (Kumar et al., 2010). A study by Wang *et al.* showed that nuclear PIP_3 bound to SF-1

accumulates to damaged DNA sites upon phosphorylation of SF1-PtdIns(4,5)P_2 by IPMK after UV irradiation. PIP_3 accumulation was further shown to mediate nuclear actin assembly and ATR recruitment. Recruitment of other DNA damage repair proteins such as MRN, Ku70-80 complex, ATM and DNA-PKcs, which are known effector proteins of PARP-1, were not affected by sequestration of PPIns, indicating that these DNA repair factors are not dependent on PPIns (Wang et al., 2017, Ray Chaudhuri and Nussenzweig, 2017). In conclusion, some of these findings could explain why no differences were observed between the MEF cells harbouring WT or kinase dead version of class I PI3K p110β. Specifically by highlighting the fact that p110β seems to have a kinase independent function in DSBR, and that PIP_3 seems to be generated by IPMK rather than p110β.

5.5 Conclusion & further perspectives

An aim of this thesis was to identify the specific PIP_3 interaction sites of PARP-1. Three PBRs or K/R motifs in PARP-1 were shown to be important for PPIn-binding. However, a limitation of this study was the use of PARP-1 fragments instead of full-length PARP-1 in the interaction studies, which may alter the overall 3D-structure. Further studies should, if possible, perform lipid overlay assay of the mutants generated in full-length PARP-1. This might not be possible due to technical difficulties in performing mutagenesis and protein expression on large multidomain proteins. Alternatively, constructs of larger PARP-1 fragments could be generated to examine if each motif influences the binding of others in a more intact protein. For example, one could generate a construct containing Znf-II, Znf-III and BRCT-domain and another construct containing the BRCT-domain, linker region and the WGR domain.

Previously, our group investigated the protein-lipid interaction between PARP-1 fragment 4 (477-524) and PIP_3 by nuclear magnetic resonance (NMR) spectroscopy. This analysis revealed that fragment 4 did bind PIP_3 and the amino acids in the K/R motif were shown to be involved in the binding. It would be interesting to perform a similar NMR analysis using PARP-1 fragment 2 (215-371) which harbours the two PBRs. This would indeed show specific interaction with PPIn.

Several studies have shown that the PBRs that bind PPIns also can be important for the site-specific localization of proteins (Viiri et al., 2009, Karlsson et al., 2016). It would therefore be

interesting to investigate whether any of the PPIn-binding sites found in PARP-1 also are necessary for its cellular localization. Especially the PBR found in the N-terminal region of zinc finger III, as it was predicted to be an NoLS in addition to binding PPIns. The mutants used in this study (see Figure 4.1) have also been generated using an N-terminal EGFP-tagged full length hPARP-1 construct. However, due to the lockdown, we did not have the time to perform the planned experiments. Right before the lockdown, we had received HeLa Kyoto WT and PARP-1 knock out (KO) cell lines from A. Mangerich, university of Constance, Germany (Veith et al., 2019)**.** The plan was to do a whole cell extract and a western blot to confirm the KO of PARP-1 in the PARP-1 KO cells. We then planned to transfect the HeLa Kyoto PARP-1 KO cells (to avoid PARP-1 overexpression) with full length, EGFP-tagged PARP-1 WT and mutants and examine their cellular localization by fluorescence microscopy.

Another aim of the study was to determine whether PIP_3 could be important for the regulation of PARP-1 enzymatic activity upon H_2O_2 induced DNA damage, as p110β and PIP_3 have been implicated in DNA repair (Kumar et al., 2010). However, no significant changes in PAR-intensities were observed between the MEF cells harbouring WT or kinase dead version of PI3K p110β. For future experiments, a few adjustments should be performed. Studies have shown that p110β and PIP_3 mediate DSB and we should therefore verify whether the H_2O_2 treatment used in this study generate DSBs or not. To do so, we could use the anti-γH2AX primary antibody for immunofluorescence studies upon the same H_2O_2 treatment, as γH2AX has been frequently used as a marker for DSB (KUO and YANG, 2008). Furthermore, as studies have shown that H_2O_2 mostly induce SSBs at the concentrations used in this study, one could consider to try out other DNA damage inducing agents such as ionizing radiation or UVA radiation which has been shown to generate DSB (Vítor et al., 2020). For example, a UVA laser micro-irradiation could be used to specifically target the nucleoli or the nucleoplasm to determine if PARP-1 is differently regulated in these two compartments upon DNA damage (Kruhlak et al., 2007).

7 References

AHMAD, Y., BOISVERT, F.-M., GREGOR, P., COBLEY, A. & LAMOND, A. I. 2009. NOPdb: Nucleolar Proteome Database--2008 update. *Nucleic acids research,* 37**,** D181-D184.

AHN, J.-Y., LIU, X., CHENG, D., PENG, J., CHAN, P.-K., WADE, P. A. & YE, K. 2005. Nucleophosmin/B23, a Nuclear PI(3,4,5)P3 Receptor, Mediates the Antiapoptotic Actions of NGF by Inhibiting CAD. *Molecular Cell,* 18**,** 435-445.

ALEMASOVA, E. E. & LAVRIK, O. I. 2019. Poly(ADP-ribosyl)ation by PARP1: reaction mechanism and regulatory proteins. *Nucleic acids research,* 47**,** 3811-3827.

ALTMEYER, M., MESSNER, S., HASSA, P. O., FEY, M. & HOTTIGER, M. O. 2009. Molecular mechanism of poly(ADP-ribosyl)ation by PARP1 and identification of lysine residues as ADP-ribose acceptor sites. *Nucleic Acids Research,* 37**,** 3723-3738.

ALVAREZ-VENEGAS, R., SADDER, M., HLAVACKA, A., BALUSKA, F., XIA, Y., LU, G., FIRSOV, A., SARATH, G., MORIYAMA, H., DUBROVSKY, J. G. & AVRAMOVA, Z. 2006. The Arabidopsis homolog of trithorax, ATX1, binds phosphatidylinositol 5-phosphate, and the two regulate a common set of target genes. *Proceedings of the National Academy of Sciences of the United States of America,* 103**,** 6049-6054.

BACKERS, K., BLERO, D., PATERNOTTE, N., ZHANG, J. & ERNEUX, C. 2003. The termination of PI3K signalling by SHIP1 and SHIP2 inositol 5-phosphatases. *Advances in Enzyme Regulation,* 43**,** 15-28.

BALLA, T. 2013. Phosphoinositides: tiny lipids with giant impact on cell regulation. *Physiological reviews,* 93**,** 1019-1137.

BARKAUSKAITE, E., JANKEVICIUS, G., LADURNER, A. G., AHEL, I. & TIMINSZKY, G. 2013. The recognition and removal of cellular poly(ADP-ribose) signals. *The FEBS Journal,* 280**,** 3491-3507.

BARLOW, C. A., LAISHRAM, R. S. & ANDERSON, R. A. 2010. Nuclear phosphoinositides: a signaling enigma wrapped in a compartmental conundrum. *Trends in Cell Biology,* 20**,** 25-35.

BARNEDA, D., COSULICH, S., STEPHENS, L. & HAWKINS, P. 2019. How is the acyl chain composition of phosphoinositides created and does it matter? *Biochemical Society transactions,* 47**,** 1291-1305.

BECK, C., ROBERT, I., REINA-SAN-MARTIN, B., SCHREIBER, V. & DANTZER, F. 2014. Poly(ADP-ribose) polymerases in double-strand break repair: Focus on PARP1, PARP2 and PARP3. *Experimental Cell Research,* 329**,** 18-25.

BILANGES, B., POSOR, Y. & VANHAESEBROECK, B. 2019. PI3K isoforms in cell signalling and vesicle trafficking. *Nature Reviews Molecular Cell Biology,* 20**,** 515-534.

BLIND, R. D., SABLIN, E. P., KUCHENBECKER, K. M., CHIU, H.-J., DEACON, A. M., DAS, D., FLETTERICK, R. J. & INGRAHAM, H. A. 2014. The signaling phospholipid PIP3 creates a new interaction surface on the nuclear receptor SF-1. *Proceedings of the National Academy of Sciences of the United States of America,* 111**,** 15054-15059.

BLIND, R. D., SUZAWA, M. & INGRAHAM, H. A. 2012. Direct modification and activation of a nuclear receptor-PIP_2 complex by the inositol lipid kinase IPMK. *Science signaling,* 5**,** ra44-ra44.

BLUNSOM, N. J. & COCKCROFT, S. 2020. Phosphatidylinositol synthesis at the endoplasmic reticulum. *Biochimica et Biophysica Acta (BBA) - Molecular and Cell Biology of Lipids,* 1865.

BOAMAH, E. K., KOTOVA, E., GARABEDIAN, M., JARNIK, M. & TULIN, A. V. 2012. Poly(ADP-Ribose) polymerase 1 (PARP-1) regulates ribosomal biogenesis in Drosophila nucleoli. *PLoS genetics,* 8**,** e1002442-e1002442.

BOCK, F. J. & CHANG, P. 2016. New directions in poly(ADP-ribose) polymerase biology. *The FEBS Journal,* 283**,** 4017-4031.

BOISVERT, F.-M., VAN KONINGSBRUGGEN, S., NAVASCUÉS, J. & LAMOND, A. I. 2007. The multifunctional nucleolus. *Nature Reviews Molecular Cell Biology,* 8**,** 574-585.

BORONENKOV, I. V., LOIJENS, J. C., UMEDA, M. & ANDERSON, R. A. 1998. Phosphoinositide signaling pathways in nuclei are associated with nuclear speckles containing pre-mRNA processing factors. *Molecular biology of the cell,* 9**,** 3547-3560.

CALDECOTT, K. W. 2008. Single-strand break repair and genetic disease. *Nature Reviews Genetics,* 9**,** 619-631.

CASTANO, E., YILDIRIM, S., FÁBEROVÁ, V., KRAUSOVÁ, A., ULIČNÁ, L., PAPRČKOVÁ, D., SZTACHO, M. & HOZÁK, P. 2019. Nuclear Phosphoinositides-Versatile Regulators of Genome Functions. *Cells,* 8**,** 649.

CHALHOUB, N. & BAKER, S. J. 2009. PTEN and the PI3-kinase pathway in cancer. *Annual review of pathology,* 4**,** 127-150.

CHEN, M., WEN, T., HORN, H. T., CHANDRAHAS, V. K., THAPA, N., CHOI, S., CRYNS, V. L. & ANDERSON, R. A. 2020. The nuclear phosphoinositide response to stress. *Cell Cycle,* 19**,** 268-289.

COCCO, L., GILMOUR, R. S., OGNIBENE, A., LETCHER, A. J., MANZOLI, F. A. & IRVINE, R. F. 1987. Synthesis of polyphosphoinositides in nuclei of Friend cells. Evidence for polyphosphoinositide metabolism inside the nucleus which changes with cell differentiation. *The Biochemical journal,* 248**,** 765-770.

COCCO, L., MARTELLI, A. M., GILMOUR, R. S., OGNIBENE, A., MANZOLI, F. A. & IRVINE, R. F. 1989. Changes in nuclear inositol phospholipids induced in intact cells by insulin-like growth factor I. *Biochemical and Biophysical Research Communications,* 159**,** 720-725.

CONSORTIUM, T. U. 2018. UniProt: a worldwide hub of protein knowledge. *Nucleic Acids Research,* 47**,** D506-D515.

CULLEN, P. J., COZIER, G. E., BANTING, G. & MELLOR, H. 2001. Modular phosphoinositide-binding domains – their role in signalling and membrane trafficking. *Current Biology,* 11**,** R882-R893.

D'AMOURS, D., DESNOYERS, S., D'SILVA, I. & POIRIER, G. G. 1999. Poly(ADP-ribosyl)ation reactions in the regulation of nuclear functions. *The Biochemical journal,* 342 (Pt 2)**,** 249-268.

DAMEN, J. E., LIU, L., ROSTEN, P., HUMPHRIES, R. K., JEFFERSON, A. B., MAJERUS, P. W. & KRYSTAL, G. 1996. The 145-kDa protein induced to associate with Shc by multiple cytokines is an inositol tetraphosphate and phosphatidylinositol 3,4,5-triphosphate 5-phosphatase. *Proceedings of the National Academy of Sciences,* 93**,** 1689.

DAWICKI-MCKENNA, J. M., LANGELIER, M.-F., DENIZIO, J. E., RICCIO, A. A., CAO, C. D., KARCH, K. R., MCCAULEY, M., STEFFEN, J. D., BLACK, B. E. & PASCAL, J. M. 2015. PARP-1 Activation Requires Local Unfolding of an Autoinhibitory Domain. *Molecular cell,* 60**,** 755-768.

DE CARVALHO, C. C. C. R. & CARAMUJO, M. J. 2018. The Various Roles of Fatty Acids. *Molecules (Basel, Switzerland),* 23**,** 2583.

DE CRAENE, J.-O., BERTAZZI, D. L., BÄR, S. & FRIANT, S. 2017. Phosphoinositides, Major Actors in Membrane Trafficking and Lipid Signaling Pathways. *International journal of molecular sciences,* 18**,** 634.

DÉLÉRIS, P., BACQUEVILLE, D., GAYRAL, S., CARREZ, L., SALLES, J.-P., PERRET, B. & BRETON-DOUILLON, M. 2003. SHIP-2 and PTEN Are Expressed and Active in Vascular Smooth Muscle Cell Nuclei, but Only SHIP-2 Is Associated with Nuclear Speckles. *Journal of Biological Chemistry,* 278**,** 38884-38891.

DI PAOLO, G. & DE CAMILLI, P. 2006. Phosphoinositides in cell regulation and membrane dynamics. *Nature,* 443**,** 651-657.

DIVECHA, N., BANFIĆ, H. & IRVINE, R. F. 1991. The polyphosphoinositide cycle exists in the nuclei of Swiss 3T3 cells under the control of a receptor (for IGF-I) in the plasma membrane, and stimulation of the cycle increases nuclear diacylglycerol and apparently induces translocation of protein kinase C to the nucleus. *The EMBO journal,* 10**,** 3207-3214.

DRAKAS, R., TU, X. & BASERGA, R. 2004. Control of cell size through phosphorylation of upstream binding factor 1 by nuclear phosphatidylinositol 3-kinase. *Proceedings of the National Academy of Sciences of the United States of America,* 101**,** 9272-9276.

EDGAR, R. C. 2004. MUSCLE: a multiple sequence alignment method with reduced time and space complexity. *BMC Bioinformatics,* 5**,** 113.

EHM, P., NALASKOWSKI, M. M., WUNDENBERG, T. & JÜCKER, M. 2015. The tumor suppressor SHIP1 colocalizes in nucleolar cavities with p53 and components of PML nuclear bodies. *Nucleus (Austin, Tex.),* 6**,** 154-164.

FAKAN, S., LEDUC, Y., LAMARRE, D., BRUNET, G. & POIRIER, G. G. 1988. Immunoelectron microscopical distribution of poly(ADP-ribose)polymerase in the mammalian cell nucleus. *Experimental Cell Research,* 179**,** 517-526.

FARLEY, K. I., SUROVTSEVA, Y., MERKEL, J. & BASERGA, S. J. 2015. Determinants of mammalian nucleolar architecture. *Chromosoma,* 124**,** 323-331.

FATOKUN, A. A., DAWSON, V. L. & DAWSON, T. M. 2014. Parthanatos: mitochondrial-linked mechanisms and therapeutic opportunities. *British journal of pharmacology,* 171**,** 2000-2016.

GAVGANI, F. M., KARLSSON, T., TANGEN, I. L., PAPDINÉ MOROVICZ, A., ARNESEN, V. S., TURCU, D. C., KRAKSTAD, C., GUILLERMET-GUIBERT, J. & LEWIS, A. E. 2019. Nuclear upregulation of PI3K p110β correlates with increased rRNA transcription in endometrial cancer cells. *bioRxiv***,** 2019.12.20.884122.

GELATO, KATHY A., TAUBER, M., ONG, MICHELLE S., WINTER, S., HIRAGAMI-HAMADA, K., SINDLINGER, J., LEMAK, A., BULTSMA, Y., HOULISTON, S., SCHWARZER, D., DIVECHA, N., ARROWSMITH, CHERYL H. & FISCHLE, W. 2014. Accessibility of Different Histone H3-Binding Domains of UHRF1 Is Allosterically Regulated by Phosphatidylinositol 5-Phosphate. *Molecular Cell,* 54**,** 905-919.

GOZANI, O., KARUMAN, P., JONES, D. R., IVANOV, D., CHA, J., LUGOVSKOY, A. A., BAIRD, C. L., ZHU, H., FIELD, S. J., LESSNICK, S. L., VILLASENOR, J., MEHROTRA, B., CHEN, J., RAO, V. R., BRUGGE, J. S., FERGUSON, C. G., PAYRASTRE, B., MYSZKA, D. G., CANTLEY, L. C., WAGNER, G., DIVECHA, N., PRESTWICH, G. D. & YUAN, J. 2003. The PHD finger of the chromatin-associated protein ING2 functions as a nuclear phosphoinositide receptor. *Cell,* 114**,** 99-111.

GUETG, C. & SANTORO, R. 2012. Formation of nuclear heterochromatin: the nucleolar point of view. *Epigenetics,* 7**,** 811-814.

GUETG, C., SCHEIFELE, F., ROSENTHAL, F., HOTTIGER, MICHAEL O. & SANTORO, R. 2012. Inheritance of Silent rDNA Chromatin Is Mediated by PARP1 via Noncoding RNA. *Molecular Cell,* 45**,** 790-800.

GUPTE, R., LIU, Z. & KRAUS, W. L. 2017. PARPs and ADP-ribosylation: recent advances linking molecular functions to biological outcomes. *Genes & development,* 31**,** 101-126.

HAKEM, R. 2008. DNA-damage repair; the good, the bad, and the ugly. *The EMBO journal,* 27**,** 589-605.

HAMMOND, G. R. V. & BALLA, T. 2015. Polyphosphoinositide binding domains: Key to inositol lipid biology. *Biochimica et Biophysica Acta (BBA) - Molecular and Cell Biology of Lipids,* 1851**,** 746-758.

HOTTIGER, M. O., HASSA, P. O., LÜSCHER, B., SCHÜLER, H. & KOCH-NOLTE, F. 2010. Toward a unified nomenclature for mammalian ADP-ribosyltransferases. *Trends in Biochemical Sciences,* 35**,** 208-219.

HU, Y., LIU, Z. & YE, K. 2005. Phosphoinositol lipids bind to phosphatidylinositol 3 (PI3)-kinase enhancer GTPase and mediate its stimulatory effect on PI3-kinase and Akt signalings. *Proceedings of the National Academy of Sciences of the United States of America,* 102**,** 16853-16858.

ISMAIL, I. H., NYSTRÖM, S., NYGREN, J. & HAMMARSTEN, O. 2005. Activation of Ataxia Telangiectasia Mutated by DNA Strand Break-inducing Agents Correlates Closely with the Number of DNA Double Strand Breaks. *Journal of Biological Chemistry,* 280**,** 4649-4655.

JACOBSEN, R. G., MAZLOUMI GAVGANI, F., EDSON, A. J., GORIS, M., ALTANKHUYAG, A. & LEWIS, A. E. 2019. Polyphosphoinositides in the nucleus: Roadmap of their effectors and mechanisms of interaction. *Advances in Biological Regulation,* 72**,** 7-21.

JEAN, S. & KIGER, A. A. 2014. Classes of phosphoinositide 3-kinases at a glance. *Journal of cell science,* 127**,** 923-928.

JUBIN, T., KADAM, A., JARIWALA, M., BHATT, S., SUTARIYA, S., GANI, A. R., GAUTAM, S. & BEGUM, R. 2016. The PARP family: insights into functional aspects of poly (ADP-ribose) polymerase-1 in cell growth and survival. *Cell proliferation,* 49**,** 421-437.

KALASOVA, I., FÁBEROVÁ, V., KALENDOVÁ, A., YILDIRIM, S., ULIČNÁ, L., VENIT, T. & HOZÁK, P. 2016. Tools for visualization of phosphoinositides in the cell nucleus. *Histochemistry and Cell Biology,* 145**,** 485-496.

KARLSSON, T., ALTANKHUYAG, A., DOBROVOLSKA, O., TURCU, D. C. & LEWIS, A. E. 2016. A polybasic motif in ErbB3-binding protein 1 (EBP1) has key functions in nucleolar localization and polyphosphoinositide interaction. *The Biochemical journal,* 473**,** 2033-2047.

KIM, D.-S., CAMACHO, C. V., NAGARI, A., MALLADI, V. S., CHALLA, S. & KRAUS, W. L. 2019. Activation of PARP-1 by snoRNAs Controls Ribosome Biogenesis and Cell Growth via the RNA Helicase DDX21. *Molecular Cell,* 75**,** 1270-1285.e14.

KIM, M. Y., ZHANG, T. & KRAUS, W. L. 2005. Poly(ADP-ribosyl)ation by PARP-1: 'PAR-laying' NAD+ into a nuclear signal. *Genes Dev,* 19**,** 1951-67.

KO, H. L. & REN, E. C. 2012. Functional Aspects of PARP1 in DNA Repair and Transcription. *Biomolecules,* 2**,** 524-548.

KOH, D. W., DAWSON, T. M. & DAWSON, V. L. 2005. Mediation of cell death by poly(ADP-ribose) polymerase-1. *Pharmacological Research,* 52**,** 5-14.

KORGAONKAR, C., HAGEN, J., TOMPKINS, V., FRAZIER, A. A., ALLAMARGOT, C., QUELLE, F. W. & QUELLE, D. E. 2005. Nucleophosmin (B23) targets ARF to nucleoli and inhibits its function. *Molecular and cellular biology,* 25**,** 1258-1271.

KRIPLANI, N., HERMIDA, M. A., BROWN, E. R. & LESLIE, N. R. 2015. Class I PI 3-kinases: Function and evolution. *Advances in Biological Regulation,* 59**,** 53-64.

KRISHNAKUMAR, R. & KRAUS, W. L. 2010. The PARP Side of the Nucleus: Molecular Actions, Physiological Outcomes, and Clinical Targets. *Molecular Cell,* 39**,** 8-24.

KRUHLAK, M., CROUCH, E. E., ORLOV, M., MONTAÑO, C., GORSKI, S. A., NUSSENZWEIG, A., MISTELI, T., PHAIR, R. D. & CASELLAS, R. 2007. The ATM repair pathway inhibits RNA polymerase I transcription in response to chromosome breaks. *Nature,* 447**,** 730-734.

KRYLOVA, I. N., SABLIN, E. P., MOORE, J., XU, R. X., WAITT, G. M., MACKAY, J. A., JUZUMIENE, D., BYNUM, J. M., MADAUSS, K., MONTANA, V., LEBEDEVA, L., SUZAWA, M., WILLIAMS, J. D., WILLIAMS, S. P., GUY, R. K., THORNTON, J. W., FLETTERICK, R. J., WILLSON, T. M. & INGRAHAM, H. A. 2005. Structural Analyses Reveal Phosphatidyl Inositols as Ligands for the NR5 Orphan Receptors SF-1 and LRH-1. *Cell,* 120**,** 343-355.

KUMAR, A., FERNANDEZ-CAPETILLO, O. & CARRERA, A. C. 2010. Nuclear phosphoinositide 3-kinase beta controls double-strand break DNA repair. *Proceedings of the National Academy of Sciences of the United States of America,* 107**,** 7491-7496.

KUMAR, A., REDONDO-MUÑOZ, J., PEREZ-GARCÍA, V., CORTES, I., CHAGOYEN, M. & CARRERA, A. C. 2011. Nuclear but not cytosolic phosphoinositide 3-kinase beta has an essential function in cell survival. *Molecular and cellular biology,* 31**,** 2122-2133.

KUO, L. J. & YANG, L.-X. 2008. γ-H2AX - A Novel Biomarker for DNA Double-strand Breaks. *In Vivo,* 22**,** 305-309.

KAADIGE, M. R. & AYER, D. E. 2006. The Polybasic Region That Follows the Plant Homeodomain Zinc Finger 1 of Pf1 Is Necessary and Sufficient for Specific Phosphoinositide Binding. *Journal of Biological Chemistry,* 281**,** 28831-28836.

LANGELIER, M., SERVENT, K., ROGERS, E. & PASCAL, J. 2008. A Third Zinc-binding Domain of Human Poly(ADP-ribose) Polymerase-1 Coordinates DNA-dependent Enzyme Activation. *The Journal of Biological Chemistry,* 283**,** 4105-4114.

LANGELIER, M.-F., PLANCK, J. L., ROY, S. & PASCAL, J. M. 2011. Crystal structures of poly(ADP-ribose) polymerase-1 (PARP-1) zinc fingers bound to DNA: structural and functional insights into DNA-dependent PARP-1 activity. *The Journal of biological chemistry,* 286**,** 10690-10701.

LANGELIER, M.-F., PLANCK, J. L., ROY, S. & PASCAL, J. M. 2012. Structural Basis for DNA Damage–Dependent Poly(ADP-ribosyl)ation by Human PARP-1. *Science,* 336**,** 728.

LÉGER, K., BÄR, D., SAVIĆ, N., SANTORO, R. & HOTTIGER, M. O. 2014. ARTD2 activity is stimulated by RNA. *Nucleic acids research,* 42**,** 5072-5082.

LEWIS, A. E., SOMMER, L., ARNTZEN, M. Ø., STRAHM, Y., MORRICE, N. A., DIVECHA, N. & D'SANTOS, C. S. 2011. Identification of nuclear

phosphatidylinositol 4,5-bisphosphate-interacting proteins by neomycin extraction. *Molecular & cellular proteomics : MCP,* 10**,** M110.003376-M110.003376.

LI, P., WANG, D., LI, H., YU, Z., CHEN, X. & FANG, J. 2014. Identification of nucleolus-localized PTEN and its function in regulating ribosome biogenesis. *Molecular Biology Reports,* 41**,** 6383-6390.

LI, Y.-P., BUSCH, R. K., VALDEZ, B. C. & BUSCH, H. 1996. C23 Interacts with B23, A Putative Nucleolar-Localization-Signal-Binding Protein. *European Journal of Biochemistry,* 237**,** 153-158.

LINDSAY, Y., MCCOULL, D., DAVIDSON, L., LESLIE, N. R., FAIRSERVICE, A., GRAY, A., LUCOCQ, J. & DOWNES, C. P. 2006. Localization of agonist-sensitive PtdIns(3,4,5)P₃ reveals a nuclear pool that is insensitive to PTEN expression. *Journal of Cell Science,* 119**,** 5160.

LINDSTRÖM, M. S., JURADA, D., BURSAC, S., ORSOLIC, I., BARTEK, J. & VOLAREVIC, S. 2018. Nucleolus as an emerging hub in maintenance of genome stability and cancer pathogenesis. *Oncogene,* 37**,** 2351-2366.

LUO, X. & KRAUS, W. L. 2012. On PAR with PARP: cellular stress signaling through poly(ADP-ribose) and PARP-1. *Genes & development,* 26**,** 417-432.

MADEIRA, F., PARK, Y. M., LEE, J., BUSO, N., GUR, T., MADHUSOODANAN, N., BASUTKAR, P., TIVEY, A. R. N., POTTER, S. C., FINN, R. D. & LOPEZ, R. 2019. The EMBL-EBI search and sequence analysis tools APIs in 2019. *Nucleic acids research,* 47**,** W636-W641.

MAEHAMA, T. & DIXON, J. E. 1998. The Tumor Suppressor, PTEN/MMAC1, Dephosphorylates the Lipid Second Messenger, Phosphatidylinositol 3,4,5-Trisphosphate. *Journal of Biological Chemistry,* 273**,** 13375-13378.

MALUCHENKO, N. V., KULAEVA, O. I., KOTOVA, E. Y., CHUPYRKINA, A. A., NIKITIN, D. V., KIRPICHNIKOV, M. P. & STUDITSKY, V. M. 2015. Molecular mechanisms of transcriptional regulation by Poly(ADP-ribose) polymerase 1. *Molecular Biology,* 49**,** 86-98.

MAO, Y. S., ZHANG, B. & SPECTOR, D. L. 2011. Biogenesis and function of nuclear bodies. *Trends in genetics : TIG,* 27**,** 295-306.

MARQUÉS, M., KUMAR, A., POVEDA, A. M., ZULUAGA, S., HERNÁNDEZ, C., JACKSON, S., PASERO, P. & CARRERA, A. C. 2009. Specific function of phosphoinositide 3-kinase beta in the control of DNA replication. *Proceedings of the National Academy of Sciences of the United States of America,* 106**,** 7525-7530.

MARTIN, T. F. J. 1998. PHOSPHOINOSITIDE LIPIDS AS SIGNALING MOLECULES: Common Themes for Signal Transduction, Cytoskeletal Regulation, and Membrane Trafficking. *Annual Review of Cell and Developmental Biology,* 14**,** 231-264.

MAZLOUMI GAVGANI, F., LEWIS, A. E. & AASLAND, R. 2017. *Nucleolar roles of the PI3K pathway in cancer and differentiation.*

MCCREA, H. J. & DE CAMILLI, P. 2009. Mutations in Phosphoinositide Metabolizing Enzymes and Human Disease. *Physiology,* 24**,** 8-16.

MCSTAY, B. 2016. Nucleolar organizer regions: genomic 'dark matter' requiring illumination. *Genes & development,* 30**,** 1598-1610.

MEDER, V. S., BOEGLIN, M., DE MURCIA, G. & SCHREIBER, V. 2005. PARP-1 and PARP-2 interact with nucleophosmin/B23 and accumulate in transcriptionally active nucleoli. *Journal of Cell Science,* 118**,** 211.

MELLMAN, D. L., GONZALES, M. L., SONG, C., BARLOW, C. A., WANG, P., KENDZIORSKI, C. & ANDERSON, R. A. 2008. A PtdIns4,5P2-regulated nuclear poly(A) polymerase controls expression of select mRNAs. *Nature,* 451**,** 1013-1017.

MOSGOELLER, W., STEINER, M., HOZAK, P., PENNER, E. & WESIERSKA-GADEK, J. 1996. Nuclear architecture and ultrastructural distribution of poly(ADP-ribosyl)transferase, a multifunctional enzyme. *Journal of Cell Science,* 109**,** 409.

MUELLER-DIECKMANN, C., KERNSTOCK, S., LISUREK, M., VON KRIES, J. P., HAAG, F., WEISS, M. S. & KOCH-NOLTE, F. 2006. The structure of human ADP-ribosylhydrolase 3 (ARH3) provides insights into the reversibility of protein ADP-ribosylation. *Proceedings of the National Academy of Sciences of the United States of America,* 103**,** 15026-15031.

NALASKOWSKI, M. M., METZNER, A., BREHM, M. A., LABIADH, S., BRAUER, H., GRABINSKI, N., MAYR, G. W. & JÜCKER, M. 2012. The inositol 5-phosphatase SHIP1 is a nucleo-cytoplasmic shuttling protein and enzymatically active in cell nuclei. *Cellular Signalling,* 24**,** 621-628.

NGUYEN, L. X. T. & MITCHELL, B. S. 2013. Akt activation enhances ribosomal RNA synthesis through casein kinase II and TIF-IA. *Proceedings of the National Academy of Sciences,* 110**,** 20681.

OKADA, M., JANG, S.-W. & YE, K. 2008. Akt phosphorylation and nuclear phosphoinositide association mediate mRNA export and cell proliferation activities by ALY. *Proceedings of the National Academy of Sciences of the United States of America,* 105**,** 8649-8654.

PAPAYANNOPOULOS, V., CO, C., PREHODA, K. E., SNAPPER, S., TAUNTON, J. & LIM, W. A. 2005. A Polybasic Motif Allows N-WASP to Act as a Sensor of PIP2 Density. *Molecular Cell,* 17**,** 181-191.

PELLETIER, J., THOMAS, G. & VOLAREVIĆ, S. 2018. Ribosome biogenesis in cancer: new players and therapeutic avenues. *Nature Reviews Cancer,* 18**,** 51-63.

PEMBERTON, J. & BALLA, T. 2018. Polyphosphoinositide-Binding Domains: Insights from Peripheral Membrane and Lipid-Transfer Proteins.

POLLOCK, C. & HUANG, S. 2010. The perinucleolar compartment. *Cold Spring Harbor perspectives in biology,* 2**,** a000679-a000679.

RAY CHAUDHURI, A. & NUSSENZWEIG, A. 2017. The multifaceted roles of PARP1 in DNA repair and chromatin remodelling. *Nature Reviews Molecular Cell Biology,* 18**,** 610-621.

RESNICK, A. C., SNOWMAN, A. M., KANG, B. N., HURT, K. J., SNYDER, S. H. & SAIARDI, A. 2005. Inositol polyphosphate multikinase is a nuclear PI3-kinase with transcriptional regulatory activity. *Proceedings of the National Academy of Sciences of the United States of America,* 102**,** 12783.

ROSENTHAL, F., FEIJS, K. L. H., FRUGIER, E., BONALLI, M., FORST, A. H., IMHOF, R., WINKLER, H. C., FISCHER, D., CAFLISCH, A., HASSA, P. O., LÜSCHER, B. & HOTTIGER, M. O. 2013. Macrodomain-containing proteins are new mono-ADP-ribosylhydrolases. *Nature Structural & Molecular Biology,* 20**,** 502-507.

ROULEAU, M., PATEL, A., HENDZEL, M. J., KAUFMANN, S. H. & POIRIER, G. G. 2010. PARP inhibition: PARP1 and beyond. *Nature reviews. Cancer,* 10**,** 293-301.

SABLIN, E. P., BLIND, R. D., UTHAYARUBAN, R., CHIU, H.-J., DEACON, A. M., DAS, D., INGRAHAM, H. A. & FLETTERICK, R. J. 2015. Structure of Liver Receptor Homolog-1 (NR5A2) with PIP3 hormone bound in the ligand binding pocket. *Journal of structural biology,* 192**,** 342-348.

SCHINDELIN, J., ARGANDA-CARRERAS, I., FRISE, E., KAYNIG, V., LONGAIR, M., PIETZSCH, T., PREIBISCH, S., RUEDEN, C., SAALFELD, S., SCHMID, B., TINEVEZ, J.-Y., WHITE, D. J., HARTENSTEIN, V., ELICEIRI, K., TOMANCAK, P. & CARDONA, A. 2012. Fiji: an open-source platform for biological-image analysis. *Nature Methods,* 9**,** 676-682.

SCHREIBER, V., AME, J. C., DOLLE, P., SCHULTZ, I., RINALDI, B., FRAULOB, V., MENISSIER-DE MURCIA, J. & DE MURCIA, G. 2002. Poly(ADP-ribose) polymerase-2 (PARP-2) is required for efficient base excision DNA repair in association with PARP-1 and XRCC1. *J Biol Chem,* 277**,** 23028-36.

SCHREIBER, V., MOLINETE, M., BOEUF, H., DE MURCIA, G. & MÉNISSIER-DE MURCIA, J. 1992. The human poly(ADP-ribose) polymerase nuclear localization signal is a bipartite element functionally separate from DNA binding and catalytic activity. *The EMBO journal,* 11**,** 3263-3269.

SCHÖFER, C. & WEIPOLTSHAMMER, K. 2018. Nucleolus and chromatin. *Histochemistry and cell biology,* 150**,** 209-225.

SCOTT, M. S., BOISVERT, F.-M., MCDOWALL, M. D., LAMOND, A. I. & BARTON, G. J. 2010. Characterization and prediction of protein nucleolar localization sequences. *Nucleic acids research,* 38**,** 7388-7399.

SCOTT, M. S., TROSHIN, P. V. & BARTON, G. J. 2011. NoD: a Nucleolar localization sequence detector for eukaryotic and viral proteins. *BMC Bioinformatics,* 12**,** 317.

SIRRI, V., URCUQUI-INCHIMA, S., ROUSSEL, P. & HERNANDEZ-VERDUN, D. 2008. Nucleolus: the fascinating nuclear body. *Histochemistry and cell biology,* 129**,** 13-31.

SLADE, D., DUNSTAN, M. S., BARKAUSKAITE, E., WESTON, R., LAFITE, P., DIXON, N., AHEL, M., LEYS, D. & AHEL, I. 2011. The structure and catalytic mechanism of a poly(ADP-ribose) glycohydrolase. *Nature,* 477**,** 616-620.

SMITH, C. D. & WELLS, W. W. 1983. Phosphorylation of rat liver nuclear envelopes. II. Characterization of in vitro lipid phosphorylation. *Journal of Biological Chemistry,* 258**,** 9368-73.

SMITH, C. D. & WELLS, W. W. 1984. Characterization of a phosphatidylinositol 4-phosphate-specific phosphomonoesterase in rat liver nuclear envelopes. *Archives of Biochemistry and Biophysics,* 235**,** 529-537.

SOBOL, M., KRAUSOVÁ, A., YILDIRIM, S., KALASOVÁ, I., FÁBEROVÁ, V., VRKOSLAV, V., PHILIMONENKO, V., MARÁŠEK, P., PASTOREK, L., ČAPEK, M., LUBOVSKÁ, Z., ULIČNÁ, L., TSUJI, T., LÍSA, M., CVAČKA, J., FUJIMOTO, T. & HOZAK, P. 2018. Nuclear phosphatidylinositol 4,5-bisphosphate islets contribute to efficient RNA polymerase II-dependent transcription. *Journal of Cell Science,* 131**,** jcs211094.

SOBOL, M., YILDIRIM, S., PHILIMONENKO, V. V., MARÁŠEK, P., CASTAÑO, E. & HOZÁK, P. 2013. UBF complexes with phosphatidylinositol 4,5-bisphosphate in nucleolar organizer regions regardless of ongoing RNA polymerase I activity. *Nucleus,* 4**,** 478-486.

SOLDANI, C. & SCOVASSI, A. I. 2002. Poly(ADP-ribose) polymerase-1 cleavage during apoptosis: An update. *Apoptosis,* 7**,** 321-328.

STAIANO, L., DE LEO, M. G., PERSICO, M. & DE MATTEIS, M. A. 2015. Mendelian disorders of PI metabolizing enzymes. *Biochimica et Biophysica Acta (BBA) - Molecular and Cell Biology of Lipids,* 1851**,** 867-881.

STIJF-BULTSMA, Y., SOMMER, L., TAUBER, M., BAALBAKI, M., GIARDOGLOU, P., JONES, D. R., GELATO, K. A., VAN PELT, J., SHAH, Z., RAHNAMOUN, H., TOMA, C., ANDERSON, K. E., HAWKINS, P., LAUBERTH, S. M., HARAMIS, A.-P. G., HART, D., FISCHLE, W. & DIVECHA, N. 2015. The basal transcription complex component TAF3 transduces changes in nuclear phosphoinositides into transcriptional output. *Molecular cell,* 58**,** 453-467.

TANAKA, K., HORIGUCHI, K., YOSHIDA, T., TAKEDA, M., FUJISAWA, H., TAKEUCHI, K., UMEDA, M., KATO, S., IHARA, S., NAGATA, S. & FUKUI, Y. 1999. Evidence That a Phosphatidylinositol 3,4,5-Trisphosphate-binding Protein Can Function in Nucleus. *Journal of Biological Chemistry,* 274**,** 3919-3922.

TANAKA, K., IMAJOH-OHMI, S., SAWADA, T., SHIRAI, R., HASHIMOTO, Y., IWASAKI, S., KAIBUCHI, K., KANAHO, Y., SHIRAI, T., TERADA, Y., KIMURA, K., NAGATA, S. & FUKUI, Y. 1997. A Target of Phosphatidylinositol 3,4,5-Trisphosphate with a Zinc Finger Motif Similar to that of the ADP-Ribosylation-Factor GTPase-Activating Protein and Two Pleckstrin Homology Domains. *European Journal of Biochemistry,* 245**,** 512-519.

TIKU, V. & ANTEBI, A. 2018. Nucleolar Function in Lifespan Regulation. *Trends in Cell Biology,* 28**,** 662-672.

ULICNA, L., KALENDOVA, A., KALASOVA, I., VACIK, T. & HOZÁK, P. 2018. PIP2 epigenetically represses rRNA genes transcription interacting with PHF8. *Biochimica et Biophysica Acta (BBA) - Molecular and Cell Biology of Lipids,* 1863**,** 266-275.

VANHAESEBROECK, B., GUILLERMET-GUIBERT, J., GRAUPERA, M. & BILANGES, B. 2010. The emerging mechanisms of isoform-specific PI3K signalling. *Nature Reviews Molecular Cell Biology,* 11**,** 329-341.

VEITH, S., SCHINK, A., ENGBRECHT, M., MACK, M., RANK, L., ROSSATTI, P., HAKOBYAN, M., GOLY, D., HEFELE, T., FRENSCH, M., FISCHBACH, A., BÜRKLE, A. & MANGERICH, A. 2019. PARP1 regulates DNA damage-induced nucleolar-nucleoplasmic shuttling of WRN and XRCC1 in a toxicant and protein-specific manner. *Scientific reports,* 9**,** 10075-10075.

VIAUD, J., MANSOUR, R., ANTKOWIAK, A., MUJALLI, A., VALET, C., CHICANNE, G., XUEREB, J.-M., TERRISSE, A.-D., SÉVERIN, S., GRATACAP, M.-P., GAITS-IACOVONI, F. & PAYRASTRE, B. 2016. Phosphoinositides: Important lipids in the coordination of cell dynamics. *Biochimie,* 125**,** 250-258.

VIIRI, K. M., JÄNIS, J., SIGGERS, T., HEINONEN, T. Y. K., VALJAKKA, J., BULYK, M. L., MÄKI, M. & LOHI, O. 2009. DNA-binding and -bending activities of SAP30L and SAP30 are mediated by a zinc-dependent module and monophosphoinositides. *Molecular and cellular biology,* 29**,** 342-356.

VINAYAGAM, A., KULKARNI, M. M., SOPKO, R., SUN, X., HU, Y., NAND, A., VILLALTA, C., MOGHIMI, A., YANG, X., MOHR, S. E., HONG, P., ASARA, J. M. & PERRIMON, N. 2016. An Integrative Analysis of the InR/PI3K/Akt Network Identifies the Dynamic Response to Insulin Signaling. *Cell reports,* 16**,** 3062-3074.

VÍTOR, A. C., HUERTAS, P., LEGUBE, G. & DE ALMEIDA, S. F. 2020. Studying DNA Double-Strand Break Repair: An Ever-Growing Toolbox. *Frontiers in Molecular Biosciences,* 7.

VYAS, S., CHESARONE-CATALDO, M., TODOROVA, T., HUANG, Y.-H. & CHANG, P. 2013. A systematic analysis of the PARP protein family identifies new functions critical for cell physiology. *Nature Communications,* 4**,** 2240.

WANG, Y.-H., HARIHARAN, A., BASTIANELLO, G., TOYAMA, Y., SHIVASHANKAR, G. V., FOIANI, M. & SHEETZ, M. P. 2017. DNA damage causes rapid accumulation of phosphoinositides for ATR signaling. *Nature Communications,* 8**,** 2118.

WEI, H. & YU, X. 2016. Functions of PARylation in DNA Damage Repair Pathways. *Genomics, Proteomics & Bioinformatics,* 14**,** 131-139.

WEN, Y., WANG, C. & HUANG, S. 2013. The perinucleolar compartment associates with malignancy. *Frontiers in biology,* 8**,** 10.1007/s11515-013-1265-z.

YILDIRIM, S., CASTANO, E., SOBOL, M., PHILIMONENKO, V. V., DZIJAK, R., VENIT, T. & HOZÁK, P. 2013. Involvement of phosphatidylinositol 4,5-bisphosphate in RNA polymerase I transcription. *Journal of Cell Science,* 126**,** 2730.

YU, F. X., SUN, H. Q., JANMEY, P. A. & YIN, H. L. 1992. Identification of a polyphosphoinositide-binding sequence in an actin monomer-binding domain of gelsolin. *Journal of Biological Chemistry,* 267**,** 14616-21.

Appendix

Amino acid sequences of GST-PARP-1 fragments (F1-6).

The sites mutated or deleted for PPIn interaction studies are highlighted in red. A mutation in fragment 1 is highlighted in yellow (see further down for explanation) and the His_6-tag for each fragment is marked in **bold**.

PARP-1 Fragment 1 (1-214):

MAESSDKLYRVEYAKSGRASCKKCSESIPKDSLRMAIMVQSPMFDGKVPHWYHFSCFWKVGHSIRHPD
VEVDGFSELRWDDQQKVKKTAEAGGVTGKGQDGIGSKAEKTLGDFAAEYAKSNRSTCKGCMEKIEK
GQVRLSKKMVGPEKPQLGMIDRWYHPGCFVKNREELGFRPEYSASQLKGFSLLATEDKEALKKQLPG
VKSEGKRKGDEVD**HHHHHH**

PARP-1 Fragment 2 (215-371):

GVDEVAKKKSKKEKDKDSKLEKALKAQNDLIWNIKDELKKVCSTNDLKELLIFNKQQVPSGESAILDR
VADGMVFGALLPCEECSGQLVFKSDAYYCTGDVTAWTKCMVKTQTPNRKEWVTPKEFREISYLKKLK
VKKQDRIFPPETSASVAATPPPS**HHH HHH**

PARP-1 Fragment 3 (372-476):

TASAPAAVNSSASADKPLSNMKILTLGKLSRNKDEVKAMIEKLGGKLTGTANKASLCISTKKEVEKMN
KKMEEVKEANIRVVSEDFLQDVSASTKSLQELFLA**HHHHHH**

PARP-1 Fragment 4 (477-524):

HILSPWGAEVKAEPVEVVAPRGKSGAALSKKSKGQVKEEGINKSEKR**HHHHHH**

PARP-1 Fragment 5 (525-656):

MKLTLKGGAAVDPDSGLEHSAHVLEKGGKVFSATLGLVDIVKGTNSYYKLQLLEDDKENRYWIFRSW
GRVGTVIGSNKLEQMPSKEDAIEHFMKLYEEKTGNAWHSKNFTKYPKKFYPLEIDYGQDEEAVKK**HH**
HHHH

PARP-1 Fragment 6 (657-1040)

LTVNPGTKSKLPKPVQDLIKMIFDVESMKKAMVEYEIDLQKMPLGKLSKRQIQAAYSILSEVQQAVSQG
SSDSQILDLSNRFYTLIPHDFGMKKPPLLNNADSVQAKAEMLDNLLDIEVAYSLLRGGSDDSSKDPIDVN
YEKLKTDIKVVDRDSEEAEIIRKYVKNTHATTHNAYDLEVIDIFKIEREGECQRYKPFKQLHNRRLLWH
GSRTTNFAGILSQGLRIAPPEAPVTGYMFGKGIYFADMVSKSANYCHTSQGDPIGLILLGEVALGNMYE
LKHASHISKLPKGKHSVKGLGKTTPDPSANISLDGVDVPLGTGISSGVNDTSLLYNEYIVYDIAQVNLKY
LLKLKFNFKTSLW**HHHHHH**

Mutagenesis:

In the present study, mutagenesis was performed to revert mutated bases in the GST-PARP-1 constructs harboring fragment 1 and 6 which were received from the Hottinger lab (results not shown in the thesis). The fragment 1 construct harbored two mutated bases as well as an extra nucleotide had been incorporated in the sequence coding for the C-terminal His-tag, while fragment 6 harbored two mutated bases (see further down).

Both mutations were reverted back to WT for fragment 6, however, for fragment 1, only the His-tag and one of the two other reverted mutations (e.g. R125C or G145D) could be generated in the same construct. When mutagenesis was performed for the last mutation, we experienced primer insertions or no yield of purified plasmid DNA. Furthermore, the new WT constructs were expressed and purified (as shown in Figure 4.2). We also planned to perform a lipid overlay assay for GST-PARP-1 fragment 1-6 with the "new" WTs. We still had to express and purify fragment 3 and as this was planned just at the time of the lockdown, we were not able to finish these experiments.

Original constructs with mutated amino acids highlighted in yellow:

PARP-1 Fragment 1 (1-214):

MAESSDKLYRVEYAKSGRASCKKCSESIPKDSLRMAIMVQSPMFDGKVPHWYHFSCFWKVGHSIRHPD
VEVDGFSELRWDDQQKVKKTAEAGGVTGKGQDGIGSKAEKTLGDFAAEYAKSNRSTR^{125}KGCMEKIE
KGQVRLSKKMVG^{145}PEKPQLGMIDRWYHPGCFVKNREELGFRPEYSASQLKGFSLLATEDKEALKKQL
PGVKSEGKRKGDEVDHHSSSSLSGRIVTD

Mutagenesis performed:

R125C CGC→TGC

G145D GGC→GAC

His-tag: CATCATTCATCATCATCAT → CATCATCATCATCATCAT (**HHHHHH**)

PARP-1 Fragment 6 (657-1040)

LTVNPGTKSKLPKPVQG^{671}LIKMIFDVESMKKAMVEYEIDLQKMPLGKLSKRQIQAAYSILSEVQQAVS
QGSSDSQILDLSNRFYTLIPHDFGMKKPPLLNNADSVQAKAEMLDNLLDIEVAYSLLRGGSDDSSKDPID
VNYEKLKTDIKVVDRDSEEAEIIRKYVKNTHATTHNAYDLEVIDIFKIEREGECQRYKPFKQLHNRRLL
WHGSRTTNFAGILSQGLRIAPPEAPVTGYMFGKGIYFADMVSKSANYCHTP^{911}QGDPIGLILLGEVALGN
MYELKHASHISKLPKGKHSVKGLGKTTPDPSANISLDGVDVPLGTGISSGVNDTSLLYNEYIVYDIAQV
NLKYLLKLKFNFKTSLW**HHHHHH**

Mutagenesis performed:

G671D GGC→GAC

P911S CCT→ TCT